General Disclaimer

One or more of the Following Statements may affect this Document

- This document has been reproduced from the best copy furnished by the organizational source. It is being released in the interest of making available as much information as possible.

- This document may contain data, which exceeds the sheet parameters. It was furnished in this condition by the organizational source and is the best copy available.

- This document may contain tone-on-tone or color graphs, charts and/or pictures, which have been reproduced in black and white.

- This document is paginated as submitted by the original source.

- Portions of this document are not fully legible due to the historical nature of some of the material. However, it is the best reproduction available from the original submission.

D. Fitzgerald ED42

Analysis of the NASA/MSFC Airborne Doppler Lidar Results from San Gorgonio Pass California

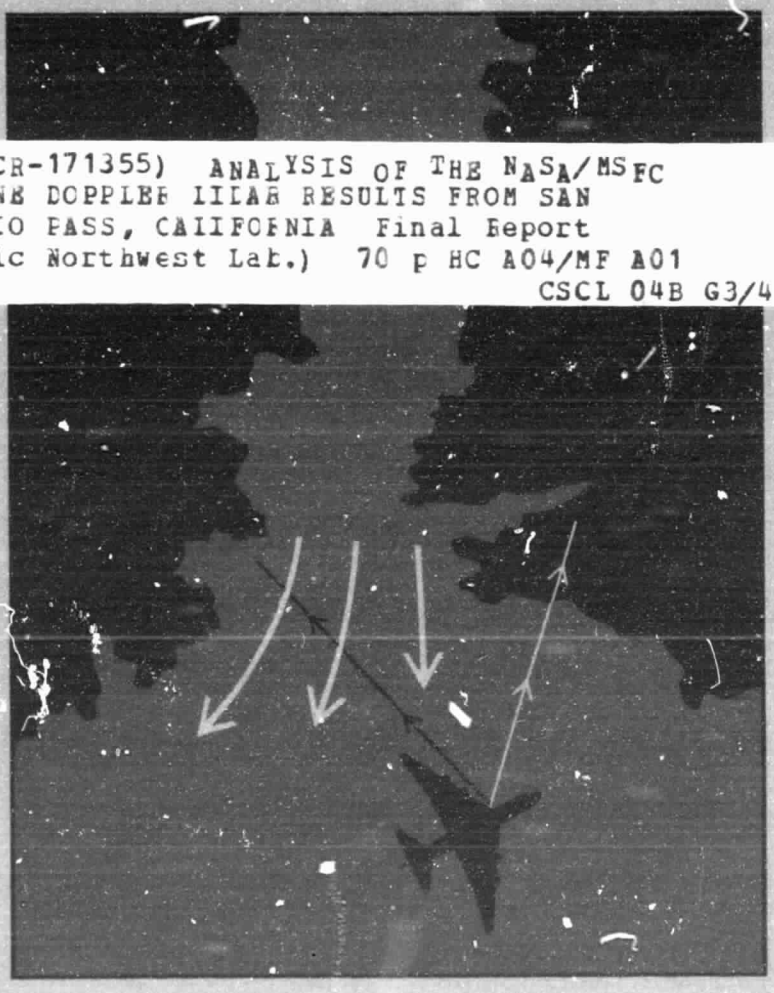

December 1984

Prepared for the National Aeronautics and Space Administration, Marshall Space Flight Center under Contract 2311104780

Battelle
Pacific Northwest Laboratories

Analysis of the NASA/MSFC Airborne Doppler Lidar Results from San Gorgonio Pass California

W. C. Cliff
J. R. Skarda
D. S. Renne
W. F. Sandusky

December 1984

Prepared for
the National Aeronautics
and Space Administration
Marshall Space Flight Center, MSFC, AL 35812
under Contract 2311104780
NASA Contract NAS8-34733

Battelle
Pacific Northwest Laboratories
Richland, Washington 99352

Acknowledgements

The authors wish to express their gratitude to Dr. James C. Dodge of the NASA HQ OSST-Mesoscale Atmospheric Processes Research Program who provided for this effort. This effort was directed and sponsored by the NASA/MSFC Atmospheric Sciences Division headed by Dr. William W. Vaughan. Dr. Dan Fitzjarrald was NASA's COR for this project and provided much direction and encouragement during the effort. Special thanks is extended to each of these individuals and the countless other NASA personnel that made these measurements possible including Dr. George H. Fichtl of NASA/MSFC, who pioneered much of the program definition; Jim Bilbro lead NASA/MSFC Doppler Lidar Engineer, Ed Weaver Principal Investigator of the NASA/MSFC Doppler Lidar Severe Storms Measurement Program, and George Alger of NASA/AMES who managed the aircraft operations.

The authors also wish to acknowledge and thank the Southern California Edison Utility for their support of this effort under the direction of Bob Yinger.

Special thanks is also acknowledged for the support the DOF Federal Wind Energy Program provided through its wind characteristic program element headed by Dr. Larry Wendell of PNL.

Executive Summary

Two days during July of 1981 the NASA/MSFC Airborne Doppler Lidar System (ADLS) was flown aboard the NASA/AMES Convair 990 on the east side of San Gorgonio Pass California, near Palm Springs, to measure and investigate the accelerated atmospheric wind field discharging from the pass.

The ADLS used a pulsed CO_2 laser with a 10.6 μm wavelength. The pulse repetition rate was 140 times a second with a 2μ sec pulse length. The return, from the laser light scattered by naturally occurring aerosols, was gated to give a spatial resolution of approximately 300 meters. The Doppler frequency shift of the returned light is a measure of the along axis component of the atmospheric velocity field. The two dimensional horizontal wind field was observed by rotating the beam first to an angle of 20^{o} in front of a normal to the aircraft, then to an angle of 20^{o} behind a normal to the aircraft, both in a horizontal plane. This technique produced a cross hatched (checkerboard) spatial picture of the horizontal wind field at each location where the path of a forward pulse and the path of a rearward pulse crossed. The two along axis component velocities measured at each pulse path crossing were used to produce a horizontal wind field. The vectors are a checkerboard spatially separated, both parallel and normal to the aircraft flight path, at about 300 meters.

These tests were conducted to examine the vertical and horizontal extent of the fast moving atmospheric flow discharging from the San Gorgonio Pass. Conventional ground measurements were also taken during the tests to assist in validating the ADLS results. This particular region is recognized as a high wind resource region and, as such, a knowledge of the horizontal and vertical extent of this flow was of interest for wind energy applications. The statistics of the atmospheric flow field itself as it discharges from the pass and then spreads out over the desert were also of scientific interests. This data provided the first spatial data for ensemble averaging of spatial correlations to compute longitudinal and lateral integral length scales in the longitudinal and lateral directions for both components. (These results will be discussed later in this executive summary.)

The mean wind field was of fundamental interest. The following figure is a plot of the horizontal wind field issuing from San Gorgonio Pass, near and over Palm Springs, obtained by the ADLS system.

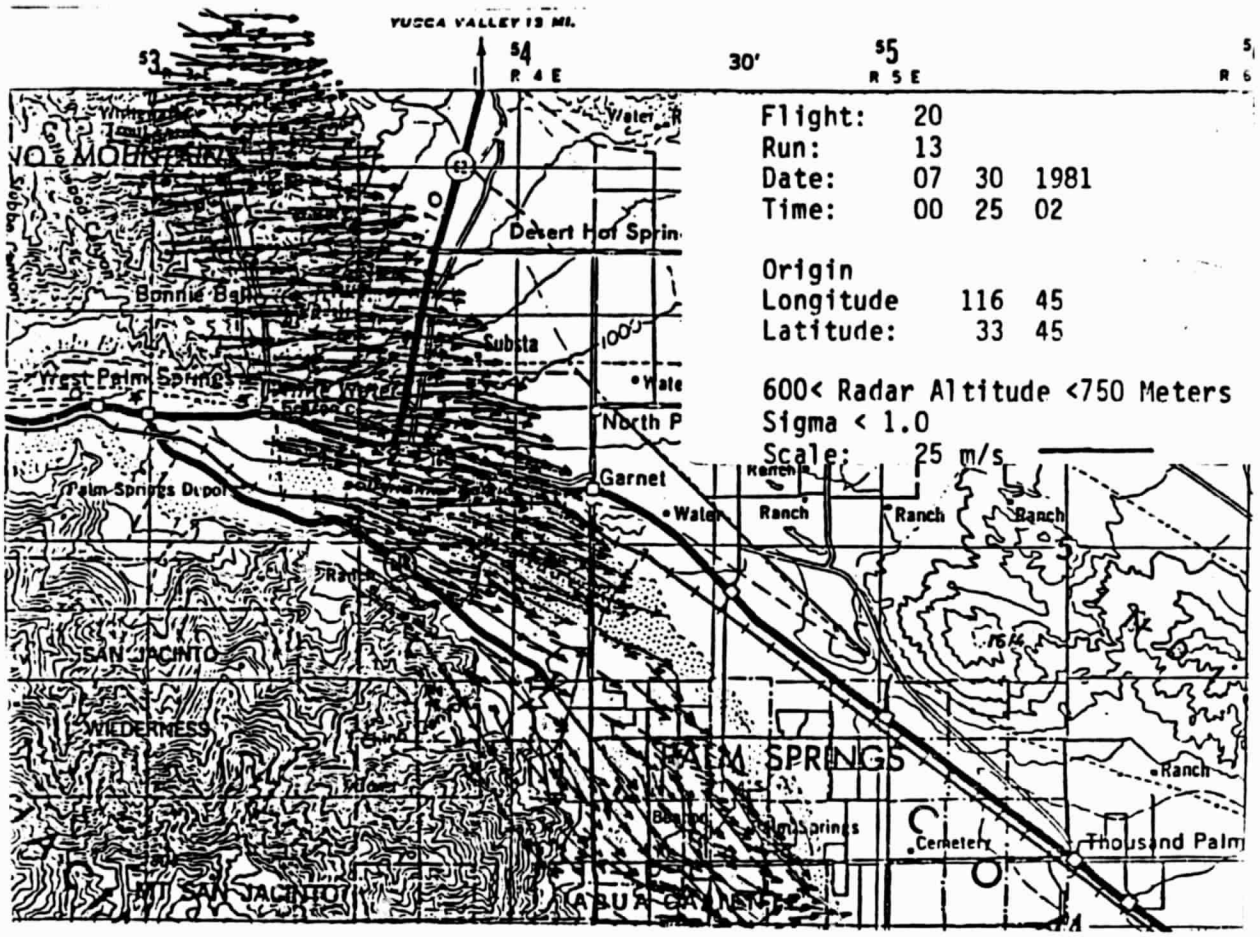

Atmospheric Wind Field Discharging From San Gorgonio Pass

The pass is near the left center of the figure, with north being at the top of the figure. The flow is seen to discharge onto the desert uniformly from the north of the pass, however, south of the pass the flow turns south and follows the mountain contours down over the Palm Springs area.

Mean winds observed with the ADLS in the vicinity of the pass were of the order of 13 m/s at an elevation of about 700 meters above grade. Ground truth

data taken from towers indicated a wind speed of approximately 13 m/s at 46 meters and kite data taken at 100 meters also indicated a wind speed of approximately 13 m/s. Power law profiles with coefficients of about 0.10 tend to exist near the ground but the profile quickly flattens and in some cases show a slightly negative exponent at higher elevations. This is as expected for accelerated and decelerated flow through a pass. The flow acceleration/deceleration provide the dominant flow effects as opposed to normal boundary layer growth from the pass floor dominating the velocity profile. The ground based tower data thus supports the ADLS data and thereby provides some validation of the ADLS mean wind data.

There has been some speculation as to whether the spread in the Doppler spectrum of the ADLS could be used as a direct measure of the turbulence within the focal volume. In an attempt to evaluate this speculation high resolution data were taken on ground towers and analyzed for times corresponding to 300 meters of wind passing over the sensors. (The 300 meters corresponds to the pulse length in which the variations from discrete particle returns would cause spread in the Doppler spectrum.) The tower data indicated a velocity RMS of approximately 1 m/s. This value was slightly larger than 1 m/s at a height of 10 meters and had fallen to about .9 m/s at a height of 46 meters. Outside of the constant shear region this value is expected to continue to decrease due to dissipation exceeding production as well as the fact that the turbulent length scale is increasing and thus the percent energy for the same high wavenumber region of interest will be less (i.e., the larger the integral scale the more energy is associated with lower wavenumbers).

The average RMS of the Doppler spread was about 1.7 m/s. There are, however, several other phenomena that contribute to the Doppler spread (e.g., the finite residence time that the scattering sources are in the sensing volume, the finite pulse length, etc.). Thus, the analysis of this test data indicates that additional thought is required before one can conclusively use the Doppler spread for assessing the turbulence level within the beam resolution volume (pulse length).

For decades scientists have estimated spatial statistics by taking time histories and then using Taylor's Hypothesis to transform the time history into a synthetic space history. Perhaps one of the greatest scientific

achievements of the ADLS system is its ability to produce a spatial field of wind vectors from which true spatial correlations and length scales may be computed.

Large areas directly at the pass exit and over Palm Springs were analyzed separately for their spatial properties. The flow over Palm Springs provides a nonaccelera ing flow field while the flow exiting the pass provides a dilitating or decelerating flow. The lateral length scale in the pass was computed to be roughly the same but slightly larger than the longitudinal length scale. (That is, the lateral component correlated in the lateral direction compared to the longitudinal component correlated in the longitudinal direction.) Over the desert near Palm Springs the traditional effect of the longitudinal length scale being the larger was observed.

The following are the authors' conclusions based upon the analysis of the NASA Airborne DLS data taken at San Gorgonio Pass.

- The NASA/ADLS measured horizontal wind fields are creditable.
- The NASA/ADLS provides unique spatial sensing of atmospheric properties previously unattainable.
- Spatial correlations and length scales have been computed at the San Gorgonio Pass exit and near Palm Springs.

The following are the authors' recommendations for future use of the NASA/ADLS.

- The NASA/ADLS be used to study flow over and about complex terrain.
- The NASA/ADLS be used to measure atmospheric flows fields to provide verification data for numerical codes used to:
  1) Predict potential dispersion of releases from nuclear power plants.
  2) Predict dispersion and concentrations of discharges from coal, gas and diesel fired turbines and power plants.

TABLE OF CONTENTS

SECTION		PAGE
	Acknowledgement.	1
	Executive Summary	2
	Table of Contents	6
	List of Tables	7
	List of Figures.	8
1.0	Historical Background	10
2.0	Introduction	12
	2.1 Region Description	12
	2.2 Doppler Lidar Description	13
3.0	Summary of Results, Conclusions and Recommendations. . .	18
4.0	Test Procedure	20
5.0	Wind Vector Analysis and Results	27
	5.1 Doppler Lidar Results	28
	5.2 Ground Truth Data	36
6.0	Correlation Analysis and Results	42
7.0	Atmospheric Length Scales	61
	Literature Cited	63
	Appendix A: Test Plan for NASA's Airborne Doppler Lidar System (ADLS) Testing in the San Gorgonio Pass Area.	64

LIST OF TABLES

TABLE NO.	TITLE	PAGE
1	Header Record for San Gogonio Flights.	24
2	Pulse Data Record.	25
3	Mean Flow Results for Run 13 and 14 (Over Palm Springs and San Gorgonio Pass). . . .	34
4	Standard Deviations of Flow Results for Run 13 and 14 (Over Palm Springs and San Gorgonio Pass) . .	35
5	Summary of Power Law Coefficients (α).	37
6	Average-Mean, RMS Turbulent Intensities for Various Elevations and Time Intervals (Approximate Space Intervals).	39
7	Integral Length Scales.	62

LIST OF FIGURES

FIGURE NO.	TITLE	PAGE
1	Block Diagram of Airborne Doppler Lidar System.	14
2	Spectral Parameters Calculated by the Signal Processor	16
3	Airborne Doppler Lidar Scan Pattern	21
4	Expanded View of Airborne Doppler Scan Pattern.	22
5	Horizontal Wind Field Exiting San Gorgonio Pass (Flight 20, Run 13, Elevation 650m)	29
6	Horizontal Wind Field Exiting San Gorgonio Pass Plotted on U.S.G.S. Topography Map (Flight 20, Run 13, Elevation 650m)	30
7	Horizontal Wind Field Exiting San Gorgonio Pass (Flight 20, Run 14, Elevation 800m)	31
8	Horizontal Wind Field Exiting San Gorgonio Pass Plotted on a U.S.G.S. Topography Map (Flight 20, Run 14, Elevation 800m)	32
9	Correlation Procedure	44
10	Average Autocorrelation of Longitudinal Component in the Longitudinal Direction over Palm Springs (Flight 20, Run 13, Elevation 650m)	45
11	Average Autocorrelation of Longitudinal Component in the Longitudinal Direction over Palm Springs (Flight 20, Run 14, Elevation 800m)	46
12	Average Autocorrelation of Longitudinal Component in the Lateral Direction over Palm Springs (Flight 20, Run 13)	47
13	Average Autocorrelation of Longitudinal Component in the Lateral Direction over Palm Springs (Flight 20, Run 14)	48
14	Average Autocorrelation of Lateral Component in the Lateral Direction over Palm Springs (Flight 20, Run 13)	49
15	Average Autocorrelation of Longitudinal Component in the Lateral Direction over Palm Springs (Flight 20, Run 14)	50

LIST OF FIGURES (continued)

FIGURE NO.	TITLE	PAGE
16	Average Autocorrelation of Longitudinal Component in the Longitudinal Direction over Palm Springs (Flight 20, Run 13)	51
17	Average Autocorrelation of Lateral Component in the Longitudinal Direction over Palm Springs (Flight 20, Run 14)	52
18	Average Autocorrelation of Longitudinal Component in the Longitudinal Direction over San Gorgonio Pass Exit (Flight 20, Run 13)	53
19	Average Autocorrelation of Longitudinal Component in the Longitudinal Direction over San Gorgonio Pass Exit (Flight 20, Run 14)	54
20	Average Autocorrelation of Longitudinal Component in the Lateral Direction over San Gorgonio Pass Exit (Flight 20, Run 13)	55
21	Average Autocorrelation of Longitudinal Component in the Lateral Direction over San Gorgonio Pass Exit (Flight 20, Run 14)	56
22	Average Autocorrelation of Lateral Component in the Lateral Direction over San Gorgonio Pass Exit (Flight 20, Run 13)	57
23	Average Autocorrelation of lateral Component in the lateral Direction over San Gorgonio Pass Exit (Flight 20, Run 14)	58
24	Average Autocorrelation of Lateral Component in the Longitudinal Direction over San Gorgonio Pass Exit (Flight 20, Run 13)	59
25	Average Autocorrelation of Lateral Component in the Longitudinal Direction over San Gorgonio Pass Exit (Flight 20, Run 14)	60

ANALYSIS OF THE NASA/MSFC AIRBORNE DOPPLER LIDAR RESULTS FROM SAN GORGONIO PASS CALIFORNIA

by
William C. Cliff
J. Raymond Skarda
David S. Renne
William Sandusky

1.0 HISTORICAL BACKGROUND

Two decades ago (1964) H. Yeh and H. Z. Cummings[1] published their experimental results which demonstrated that coherent laser systems could be used to accurately measure fluid velocities. The potential for this new technology was quickly recognized by both private industry and by the federal government labs. Similar programs/concepts that were being pursued at this same time by industry and government were accelerated and by the mid-60's private industry was marketing small laboratory systems, which by now had become known as Laser Doppler Velocimeters (LDV), with measurement sensing ranges of up to a few meters. Systems which could probe longer ranges were being pursued by government labs such as the NASA's Marshall Space Flight Center and the Airforce's Arnold Engineering and Development Center. The Arnold approach was to scale up one of the techniques which were being effectively used in the laboratory. This was a system which comprised of a laser beam being split and the recombined at the desired sensing location. Ranges of tens of meters have been achieved but the system was massive and somewhat limited in capability. Over the years several investigators have used this approach for atmospheric velocities with limited success.

At the same time a NASA team headed by Robert Milton Huffaker had been working on a unique approach which used a continuous wave (CW) CO_2 single beam laser system which transmitted the laser light and received the returned light along the same optical path (coaxial).

In the 1966-67 time frame the first signal return were measured with the CW-CO_2 coaxial system. Due to the the focal volume increasing with increasing focal distance the range of this system is limited to about 400 meters.

Because many atmospheric applications require sensing at ranges greater than 500 meters, the design of a coaxial CO_2 pulsed system was developed at NASA/MSFC from 1968 to 1970. The system was first designed to look forward from an aircraft to detect Clear Air Turbulence (CAT). The pulsed system was fabricated and flown in 1972 and 1974 on the NASA/AMES Airborne Laboratory, a convair 990 aircraft named Galileo. The CAT system was managed by Ed Weaver of NASA/MSFC, while Galileo was managed by Herb Cross NASA/AMES. Two months after the 1974 flight testing of the CAT system, a navy subchaser and the Galileo collided in mid-air taking the lives of all on board the Galileo. During the next few years NASA/AMES equipped another Convair 990 to become their new flying laboratory name Galileo II that carried the CAT system on a 1979 mission. NASA/MSFC continued the development of both their CW and pulsed CO_2 coaxial Laser Doppler Systems.

The pulsed system was improved and a scanning system was developed which would tie directly into the inertial navigation system of the Galileo II. During this period the development and use of NASA/MSFC Laser Doppler Systems were under Dr. William W. Vaughan and Dr. G. H. Fichtl with Ed Weaver still managing the airborne system and Jim Bilbro becoming the lead engineer.

By 1981 the new scanning Airborne Laser Doppler System (now known as Airborne Doppler Lidar) was ready for collecting data on the first set of scientific experiments with Dr. Dan Fitzjarrald in charge of the experiments which had been proposed by private industry, universities and other government agencies. The Airborne Doppler Lidar System was fitted into the Galileo II in June 1981 to perform tests associated with Dr. James Dodge's (NASA HQ) severe storms program. The NASA/MSFC team was the same as given above and the Galileo was now managed by George Alger as it was for the 1979 CAT flights.

During June and July of 1981 the Galileo would perform 21 flights which employed the Airborne Doppler Lidar.[2] On two of these flights, July 10 and July 29, the Airborne Doppler Lidar System measured the wind field exiting the east end of San Gorgonio Pass, California. It is these tests and the analysis of the Airborne Doppler Wind Data that are the subject of this report.

2.0 INTRODUCTION

2.1 Region Description

The San Gorgonio Pass region was identified in October 1980 by NASA's Secondary Flows, Boundary Layers, Turbulence, Wave Team, as a region where the atmospheric flow field was of scientific and practical significance and interest. The San Gorgonio Pass is located approximately 200 Km (120 miles) east of Los Angeles. The pass is about 40 Km (25 miles) long with a westerly elevation of approximately 760 m (2500 ft) gradually dropping to an elevation of approximately 200 m (700 ft). The width of the pass is roughly 8 Km (5 miles)[at a contour approximately 300 m (1000 ft) above the pass floor]. The east end the pass quickly broadens and becomes open desert floor. The mountains through which the pass penetrates rise to about 3350 Km (11,000 ft) within 16 to 24 Km (10-15 miles) on each side of the pass floor. When the marine inversion layer on the Los Angeles side builds to a depth greater than the pass entrance elevation, the marine air begins flowing down the pass. The flow is accelerated into and down the pass and then decelerates as it expands onto the desert on the east side.

This region is well known for its extraordinarily strong winds and was considered to potentially be a strong wind resource location. However for the region to be a strong wind source location for multiple wind turbines spaced in a direction parallel to the prevailing wind direction (aligned with the pass), the high winds must be more than just strong surface winds. The strong winds must extend to significant heights above grade level. This is so that there would be sufficient upper air momentum to replace the momentum extracted by upwind wind turbines. This vertical extend of these strong winds along with the spreading of these strong winds over the valley floor were the practical interests of this atmospheric region.

Scientific objectives which were to be met by investigation of this region were the examination of the atmospheric flow field as it diverged at the pass exit and the comparison of these results with those obtained over the desert region where the streamlines become straight and parallel. Since this would be the first opportunity to examine detailed spatial wind fields in the boundary layer, this region presented a unique opportunity to examine spatial

correlations, both lateral and longitudinal at upper elevations for both the diverging pass flow as well as over the desert floor. Other scientific items of interest were to compare Doppler Lidar results with data obtained from terrestrial measuring systems such as met towers equipped with conventional anemometers and kites. Several of the other Airborne Doppler Lidar experiments flown during the June-July 1981 time frame were also established for comparing the Airborne Doppler Lidar results with those obtained by other measuring techniques such as Dual Doppler Radar with chaff as a tracer and small plane measurements. Since all tower and kite type data provide only temporal information, comparisons of the Doppler Lidar Data with tower or kite data do require that time and space statistics be related through Taylors hypothesis[3] which states in part that "...one may assume that the sequence of changes in u at a fixed point are simply due to the passage of an unchanging pattern of turbulent motion over the point, i.e., one may assume u = $\Phi(t) = \Phi(x/U)$ where x is measured upstream at time t=0 from the fixed point where u is measured." Where u is the fluctuating portion of the velocity, U the mean velocity and t is time. With temporal and spatial mean velocities being comparable by considering stationarity and continuity.

2.2 Airborne Doppler Lidar Description

The following description of the Airborne Doppler Lidar System used in the San Gorgonio experiment is for the most part extracted from reference 2 courtesy of Jim Bilbro. A block diagram of the Airborne Doppler Lidar System (ADLS) is provided in figure 1.

The master oscillator is a small, 8 W continuous wave CO_2 laser operating at a wavelength of 10.6 μm. A beam splitter permits a small portion of the output of this laser to be used as a local oscillator which is shifted in polarization by 90^0 (not shown in Figure 1) then recombined with the scattered return creating a time dependent interference pattern on a light sensitive detector. The major portion of the laser beam is directed through an electro-optic modulator, where it is amplitude-modulated to form a train of 2 μs (330 m) long pulses. This laser pulse train passes through an optical isolator, expander, and a series of six amplifier tubes.

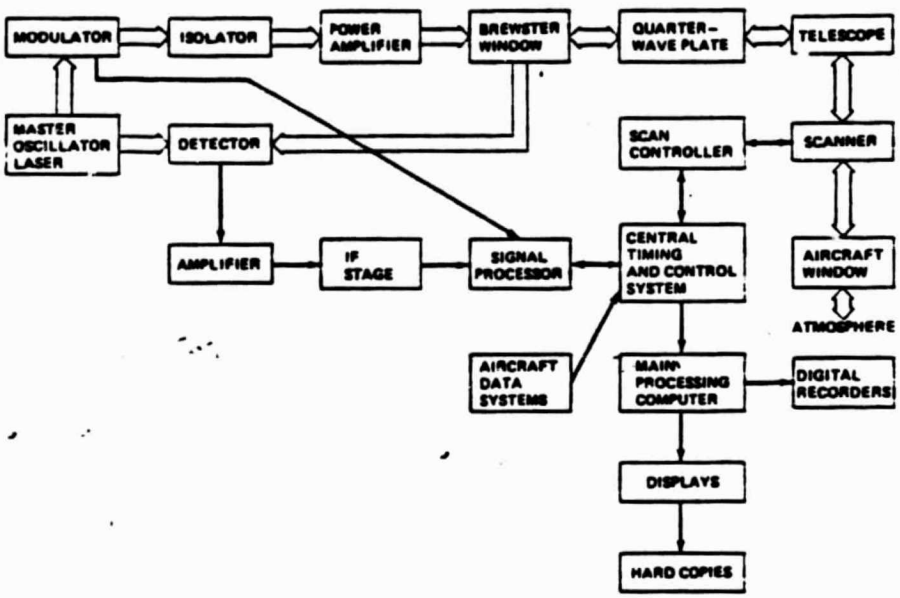

Figure 1. Block diagram of Airborne Doppler Lidar System. Broad arrows refer to light signals and single-black arrows refer to electronic signals (From Reference 2, Courtesy of J. Bilbro)

After exiting the amplifier, the laser pulses pass through a Brewster window and quarter-wave plate. The pulses are then expanded and collimated by a 30 cm, all aluminum, off-axis telescope to a diameter of 0.24 m (measured to the 2 point of the Gaussian-shaped amplitude distribution). The pulses then pass through two germanium wedges that allow scanning in a horizontal plane 20^{o} forward and 20^{o} aft of the telescope line-of-sight (which is normal to the aircraft centerline). The pulses exit the aircraft through a germanium window, which also serves as a pressure bulkhead. Once the pulses enter the atmosphere, their light is scattered in all directions by aerosols typically ranging from 1 to 10 μm in diameter. Some of the radiation is scattered back along the axis of illumination, having been both phase and frequency shifted. The amount that the frequency is shifted is called the Doppler shift or Doppler frequency. The Doppler shift, Δf, is proportional to the line-of-sight velocity component of the scattering sources. The equation for the Doppler shift as a function of the line-of-sight component, V_L, is: $\Delta f = 2V_L/\lambda$.

The back-scattered radiation from measurement volumes (0.24 m diameter, 330 m length) is collected by the same telescope responsible for the transmission. The radiation travels back through the quarter-wave plate to the Brewster window, where it is reflected to a beam splitter (due to the fact that at this location the returning light is polarized 90^{o} to the transmitted light and is now reflected from the Brewster window, through which the transmitted light passes). The returning radiation is then combined with the local oscillator, and focused on the surface of a liquid-nitrogen cooled HgCdTe detector. The combination of the two beams results in an interference pattern that varies in time according to the frequency difference between the local oscillator and the back-scattered radiation. The output of the detector is an FM signal, whose modulation is proportional to the Doppler shift associated with the movement of aerosols contained within the measurement volume.

The detector output is amplified, and then the frequency analyzed using a multiple band pass analyzer. At this time, three spectral parameters are extracted. These three spectral parameters are shown in Figure 2 (Lee, 1980).

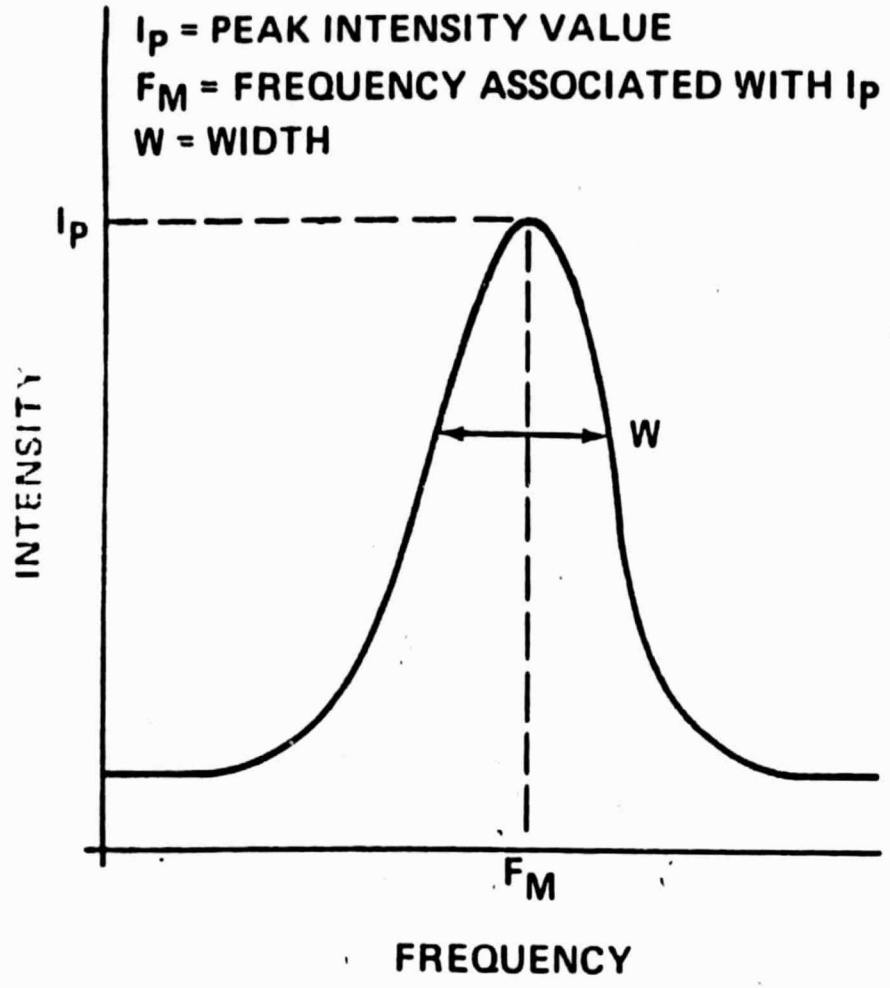

Figure 2. Spectral Parameters Calculated by the Signal Processor

The mean frequency shift is related to the mean aerosol line-of-sight velocity, while the intensity is related to the back-scattered power. The spectral width is estimated from the shape of the autocovariance by performing a least-squares fit to a Gaussian distribution. A portion of the spectral width relates to the spread in velocities in the measurement volume. Other effects also cause the spectrum to broaden, (e.g., broadening due to the fact that the data record is not infinite, broadening due to finite resonance time of the aerosols, and others).

The on board inertial navigation system provides data to the Airborne Doppler Lidar's Central Timing and Control Systems (CTCS) from which the aircrafts pitch and roll are used to control the scanner position so that the Doppler Lidar System scans only in a horizontal plane. The planes motion relative to the ground, along with the beam direction, is used to compute the Doppler frequency shift that results from the motion of the aircraft. This frequency is then removed from the return Doppler frequency prior to computation of the wind velocity.

3.0 SUMMARY OF RESULTS, CONCLUSIONS AND RECOMMENDATIONS

3.1 Results

- The NASA Airborne Doppler Lidar System successfully measured the horizontal wind field near the east side of San Gorgonio Pass, California.

- The depth of the accelerated flow from the San Gorgonio Pass was in excess of 1 KM.

- The atmospheric flow from the pass spreads out to follow the hills to the south over Palm Springs but tends to discharge easterly at the north side of the pass.

- Ground data indicate that near surface flows channel somewhat down the center of the pass.

- Spatial correlations were computed from the ADLS data exiting the pass as well as over Palm Springs.

- Integral length scales of the wind field ranged from about 300 to 500 meters at elevations of 650-800 meters.

3.2 Conclusions

- The NASA ADLS can accurately measure the horizontal wind field over complex terrain with a grid point spacing of about 300 meters with a range of about 10 KM (e.g., each pulse is sensed every 300 meters by gating the return).

- The NASA ADLS provides a unique capability for performing atmospheric research with unique spatial resolution previously unattainable.

3.3 Recommendations

- The NASA ADLS be used to study atmospheric flow fields over complex terrain.

- the NASA ADLS be used to measure atmospheric flow fields for comparison, validation and upgrading of numerical codes used to predict dispersion and concentrations from sources of concern (e.g., power plants, mining locations, etc.).

- The NASA ADLS be used as a scientific tool for investigating atmospheric turbulence and measuring atmospheric spectra and length scales over uniform terrain for various surface roughness.

- The NASA ADLS be used to study the flow behind large isolated knolls.

4.0 TEST PROCEDURES

As was mentioned previously, the ADLS alternatively scans 20^{o} forward and then 20^{o} aft. It takes approximately 0.5 seconds for the scanning operation. The length of time required for each forward or aft measurement depends upon the number of pulses one wishes to average. For the San Gorgonio flight 120 pulses were averaged for each measurement.

A 2μ second pulse was used with a repetition rate of 140 per second and a gating of the return every 2μ seconds. This enabled the system to provide wind data about every 300 meters both parallel and normal to the planes motion.

Figures 3 and 4 (courtesy J. Bilbro from Ref. 4) graphically depict the scanning process used with the Airborne Doppler Lidar System.

A flight test plan was developed which utilized the ADLS' capability for detailing the flow exiting the San Gorgonio Pass as well as flow over Palm Springs. Appendix A is a copy of the test plan conceived for the San Gorgonio tests. Ground data was to be taken at several locations throughout the San Gorgonio region, including data from:

- a 100 meter meteorological tower in the pass
- a 50 meter meteorological tower just downstream of the pass exit on the north side of the pass
- several 10 meter towers
- several tala kites.

The flight of the NASA Convair 990 was to be at elevations where the aircraft was as low as possible to collect data that was as close to the ground data as possible. The flight paths were also to be at higher elevations to determine the vertical extent of the accelerated flow through the pass.

The ADLS beam could also be locked at a slightly depressed angle enabling a one dimensional look at velocities as a function of elevation. Several flight paths incorporating this feature were also suggested in the test plan.

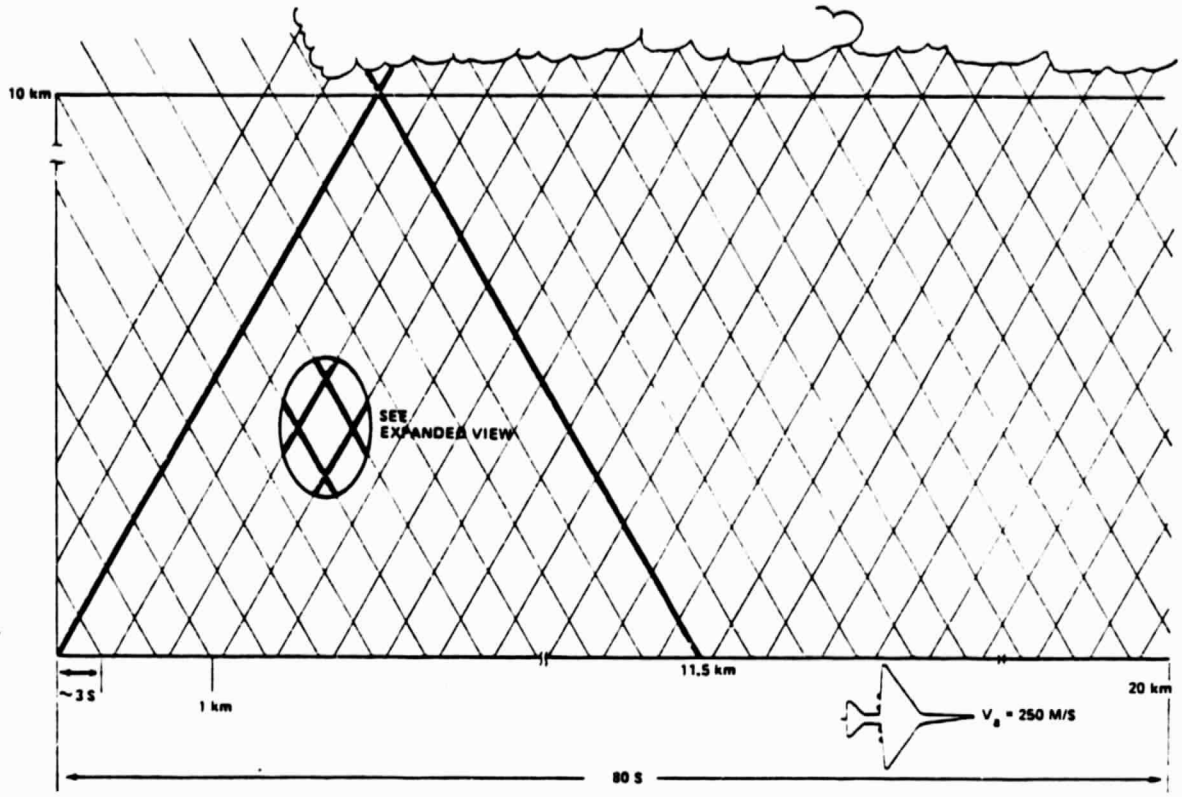

Figure 3. Airborne Doppler Lidar Scan Pattern
(Courtesy of J. Bilbro, NASA/MSFC, Reference 4)

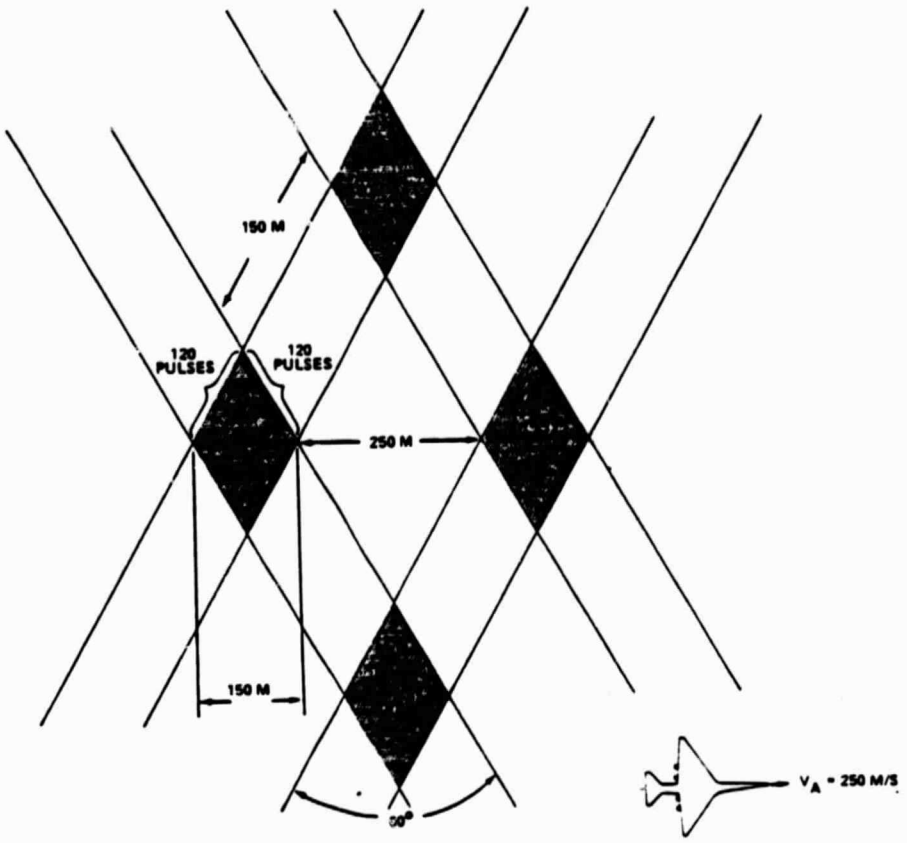

Figure 4. Expanded View of Airborne Doppler Scan Pattern
(Courtesy of J. Bilbro, NASA/MSFC, Reference 4)

Because of the tremendous amount of information being received during a test, much onboard real time data compression and computing was performed. Some additional data handling was performed at the Marshall Space Flight Center (MSFC) with the reduced data for the various tests was then distributed to the various principal investigators.

Table 1 is a listing of the information provided on the magnetic tape header record for the San Gorgonio flights, Table 2 is a listing of the information provided on the data tape for each pulse. Note that each pulse is range gated 45 times for the San Gorgonio tests. This means that the atmospheric velocity was ampled at 45 locations along each pulse.

TABLE 1. HEADER RECORD FOR SAN GORGONIO FLIGHTS

WORD #	NAME		WEIGHT
1	Flight #		1
2	Run #		1
3	Month		1
4	Day	Flight Date	1
5	Year		1
5	Hours		1
6	Minutes	Start Time	1
7	Seconds		1
8	Hours		1
9	Minutes	Stop Time	1
10	Seconds		1
11-90	Spare		

TABLE 2. PULSE DATA RECORD

WORD #	NAME	WEIGHT
1	East Distance	20m
2	North Distance	20m
3	LOS	.1°
4-11	Spare	
12	Lidar Amplitude Raw	.1875 dB
13	Lidar Velocity Raw	.08 m/s
14	Lidar Width	1 (coded)
15	East Distance	20m
16	North Distance	20m
17	S	.001
18	Lidar Amplitude Threshold and range corrected	.1875
19	Lidar Velocity*	.08 m/s
20	C_1	
21	C_2	
22	C_3 Smooth Coefficients	.0000001
23	C_4	
24	C_5	
25	C_6 Spare Coefficients	
26	C_7	
27	East Distance Advected**	20m
28	North Distance Advected**	20m
29	Vorticity	
30	Divergence	
31	Stretch	
32	Shear	
	Words 12-32 repeat 44 more times once for each Bin	
957	Flight #	1
958	Day #	1
959	Run #	1
960	Time, Seconds	.1s
961	Time, Minutes from Midnight	1m
962	Pressure Altitude	16,479 ft.
963	Spare	
964	Radar Altitude	2 ft.
965	Dew/Frost Point	.1°C
966	Static Air Temp.	.1°C
967	IR Surface Temp.	.1°C
968	Total Air Temp.	.1°C
969	Latitude, Minutes	.1 min.
970	Latitude, Degrees	1 deg.
971	Longitude, Minutes	.1 min.
972	Longitude, Degrees	1 deg.
973	True Heading	.044
974	True Air Speed	1 kts.
975	Ground Speed	.1221 kts.

TABLE 2. (continued)

WORD #	NAME	WEIGHT
976	Drift Angle	.043945°
977	Wind Speed	.1 kt
978	Wind Direction	.1°
979	Pitch	.043945°
980	Roll	.043945°
981	Wedge Angle, Inner	.1°
982	Wedge Angle, Outer	.1°
983	Time to Position	10
984	Sensor Motor Temp.	.1°C
985	LOS Elevation	.1°
986	Pulses Per Integration	1
987	Number of Lags	1
988	Track	.043945°
989	Lo Frequency	.01
990	Off-set	.08
991	Spare	

5.0 WIND VECTOR ANALYSIS AND RESULTS

The wind vector data for the San Gorgonio's test were collected using the NASA ADLS system described in Section 2.2. A resolution of about 330 meters was resolved along the lidar beam pulse by using a 0.2μ sec pulse of the laser and gating the return every 2.13μ sec. The returned radiation is attributed primarily to back scattering by aerosols ranging from 1 to 10μm in diameter. The difference between the frequencies of the transmitted and received radiation are a linear measure of the radial (along beam) component of velocity. This relation is given by: $V_{radial} = C\ \Delta f$

where: V_{radial} = radial (along beam) component of the atmospheric velocity
C = $2/\lambda$ where λ is 10.6μm (the wavelength of the laser)
Δf = the Doppler frequency (frequency difference of the transmitted and received radiation).

The measurement volume (for each pulse) is a cylindrical region bound by the pulse diameter and the resolution length R. R is approximated by: R= 1/2CT

where: C = speed of light ($3x10^8$ m/s)
T = Duration of receiver gate (2.13 s)

The factor 1/2, comes about by convolving the pulse length and the duration of the gate.

The back-scattered radiation is the incoherent sum of all the scatters within the measurement volume. Spectral analysis of the measurement volume signal was performed on board the aircraft using the following three spectral parameters: (a) mean doppler frequency, (b) intensity of return, and (c) spectral width as described in Section 2.2. These parameters were averaged over 140 pulses to get a mean spatial average along the flight path as well as normal to the flight path.

The doppler lidar beam directions were 20^o forward and 20^o aft of a direction normal to the aircraft. The locations where a forward beam sampled the atmosphere and subsequently the rearward beam sampled the atmosphere are locations where the horizontal wind vector was computed.

5.1 Doppler Lidar Results

The horizontal wind fields for the San Gorgonio ADLS tests were measured using the techniques described in Section 2.2 and 5.0. The following results are those obtained from NASA Flight 20, runs 13 and 14 which were performed on July 29, 1981. The atmospheric horizontal wind fields from runs 13 are shown in Figure 5 and 6 and the horizontal wind fields from run 14 are shown in Figures 7 and 8.

Figure 5 shows only the measured horizontal wind field for run 13 while Figure 6 shows the measured horizontal wind field plotted on a USGS topographic map of the area. Similarly, Figure 7 is only the measured horizontal wind field for run 14 while Figure 8 is the horizontal wind field for run 14 superimposed on a USGS topographic map of the area. The ability to overlay the horizontal wind field over a USGS topographic map is made possible because the NASA ADLS system is tied to the aircrafts inertial navigation system. From the knowledge of exactly where the plane is and a knowledge of the beam configuration relative to the plane, the location of each measurement volume along each pulse is determined very accurately. It is perhaps at this location in the report that one begins seeing the extreme sophistication and potential worth of this state-of-the-art system.

A more detailed examination of the data was performed on both runs in the regions of the flow issuing from the pass and the flow over Palm Springs. These regions were examined in terms of their mean flow characteristics, averaged autocorrelations, and corresponding integral length scales.

The correlation analysis will be presented in Section 6.0 and the integral length scales for all horizontal components and directions are presented in Section 7.0.

The location of the two regions of interest where extensive analysis was performed is as follows:

San Gorgonio Pass: 14,000 to 21,000 meters N
11,000 to 21,000 meters E

Palm Springs: 6,800 to 13,000 meters N
13,900 to 24,300 meters E

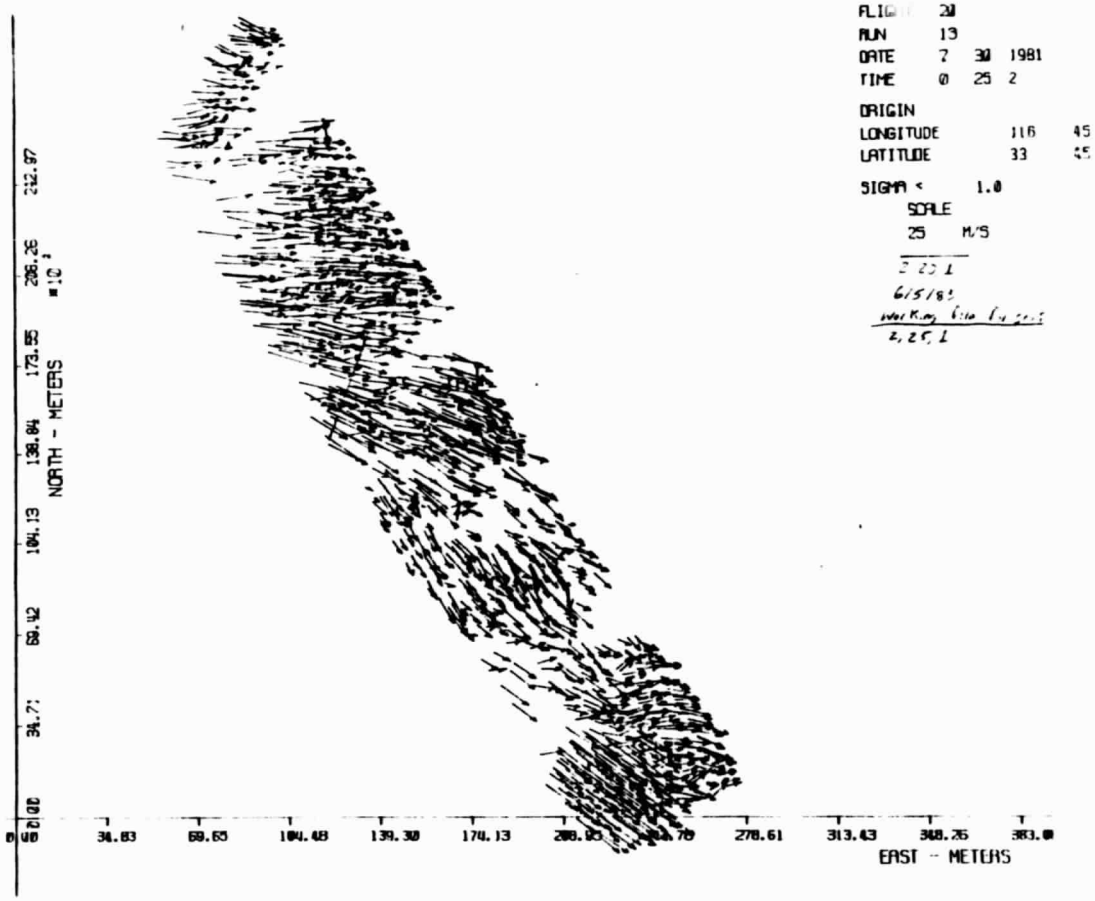

FIGURE 5. Horizontal Wind Field Exiting San Gorgonio Pass (Flight 20, Run 13, Elevation 650 m)

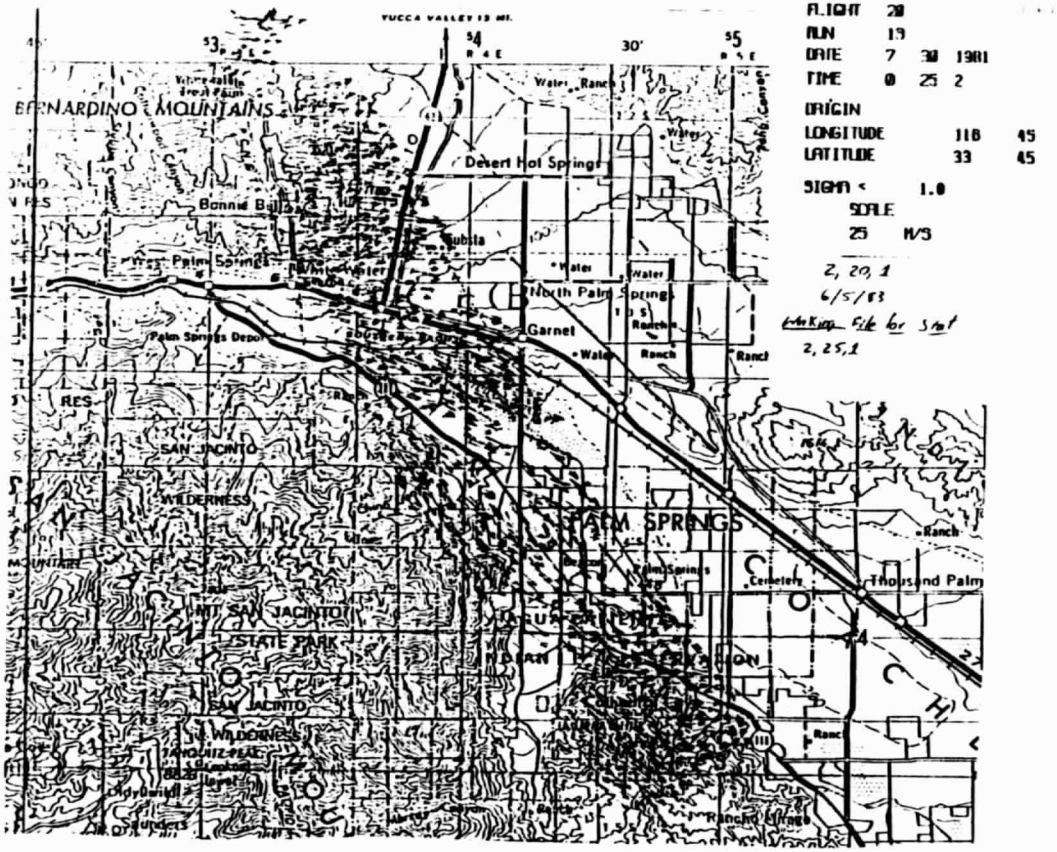

FIGURE 6. Horizontal Wind Field Exiting San Gorgonio Pass Plotted on U.S.G.S. Topography Map (Flight 20, Run 13, Elevation 650 m)

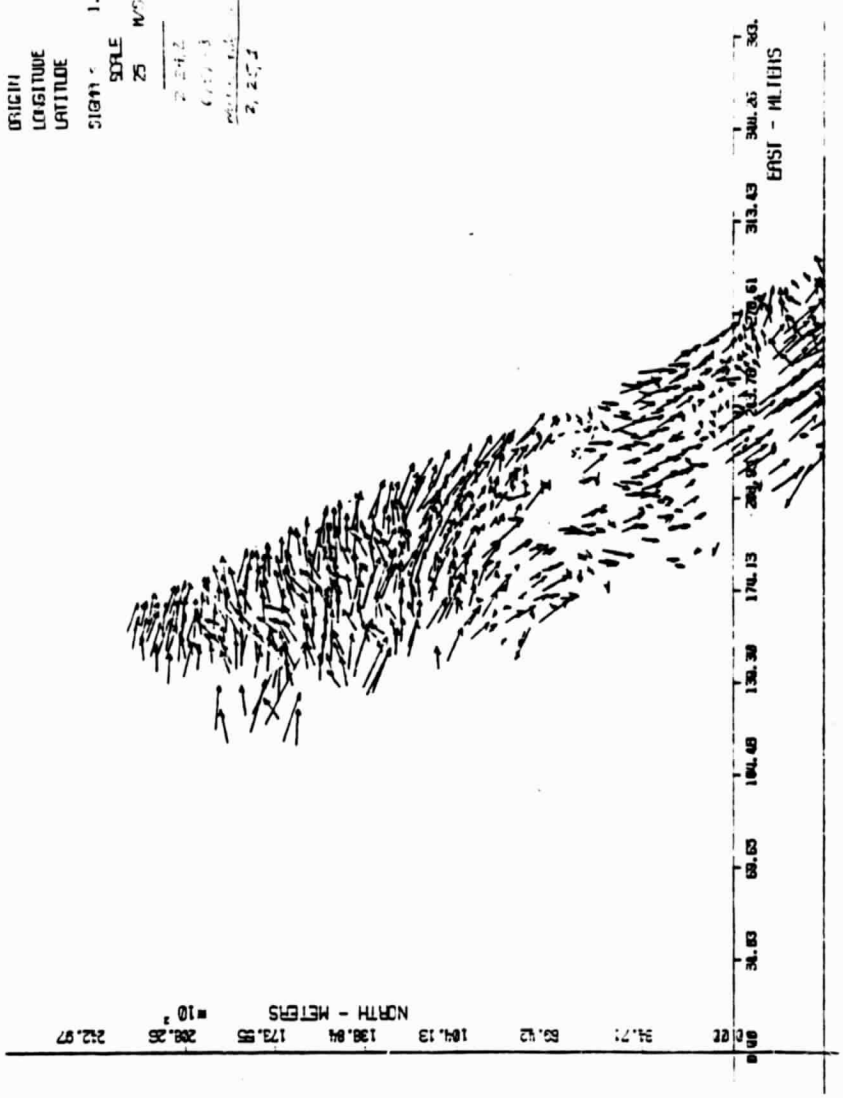

FIGURE 7. Horizontal Wind Field Exiting San Gorgonio Pass (Flight 20, Run 14, Elevation 800 m)

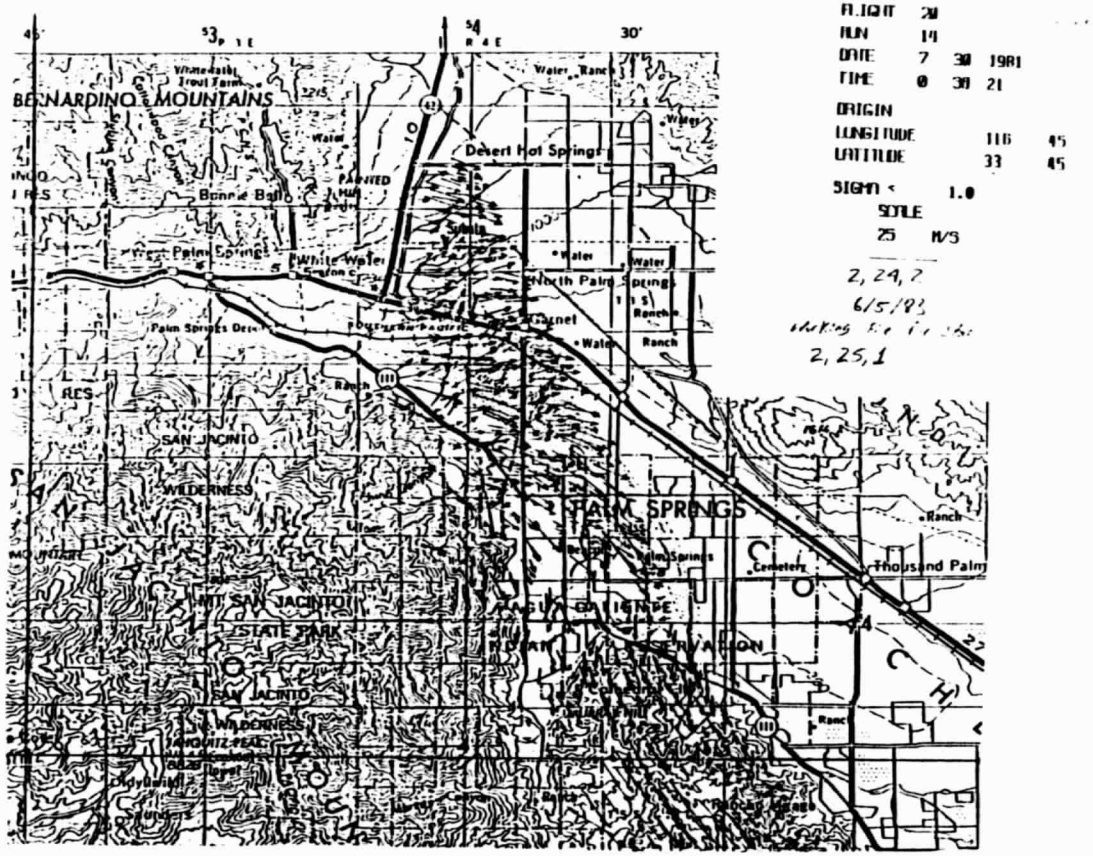

FIGURE 8. Horizontal Wind Field Exiting San Gorgonio Pass Plotted on a U.S.G.S. Topography Map (Flight 20, Run 14, Elevation 800 m)

The above regions are defined with respect to a reference location with a latitude of $33^{o}45'$ and a longitude of $116^{o}45'$. The mean flow characteristics and standard deviation are summarized in Tables 3 and 4 respectively.

General flow observations indicate that the flow exiting from the pass has a higher velocity than the flow over Palm Springs. The lower flow velocities over the Palm Springs region relative to the flow velocities in the pass are expected (from continuity) as a result of the diverging cross sectional flow area at the exit of the pass.

On the central to north side of the pass the flow tends to exit almost due east while the flow direction over Palm Springs is 37^{o} and 22^{o} south of east for runs 13 and 14 respectively. The flow measurements were taken between 650 and 800 meters above grades, which are at higher elevations than the detailed flow/turbulence measurements of previous investigations (2, 5, 6, 7). There have of course been aircraft measurements with much poorer resolution than the ADLS system resolution.

It should be noted that prior to any formal analysis of the data, the data itself was analyzed for validity. Parameters used to screen the data and eliminate/reject bad points were pulse amplitude, velocity width (doppler spread), pulse noise level (pulse sigma value), line of sight velocity and the north and east velocity components.

In order for a data point to be accepted it had to meet the following final screening criteria:

- sigma ≥ 1.0
- amplitude ≥ 126 db
- width ≤ 6 m/s
- $|VLOS| \leq 30$ m/s
- $|V_{north}| \leq 30$ m/s
- $|V_{east}| \leq 30$ m/s

TABLE 3. MEAN FLOW RESULTS FOR RUN 13 AND 14
(Over Palm Springs and San Gorgonio Pass)

Data	Run 13 Palm Springs	Run 13 Pass Data	Run 14 Palm Springs	Run 14 Pass
Mean Flow Angle (radians with respect to east)	-.65	-.23	-.37	0.17
Mean Longitude Velocity (m/s)	6.91	12.8	7.83	9.53
Mean Lateral Velocity (m/s)	-.41	-.30	-.47	-.63
Mean Altitude (m)	709	798	643	803
Mean Amplitude (db)	141	143	141	141
Mean Sigma Value (m/s)	0.221	0.164	0.243	0.264
Mean Velocity Width (m/s)	1.71	1.76	1.80	1.44
Mean Velocity Magnitude (m/s)	7.2	13.2	8.4	10.1

TABLE 4. STANDARD DEVIATIONS OF FLOW RESULTS FOR RUN 13 AND 14 (Over Palm Springs and San Gorgonio Pass)

Data	Run 13 Palm Springs	Run 13 Pass Data	Run 14 Palm Springs	Run 14 Pass
Flow Angle (radians with respect to east)	0.38	0.22	0.48	0.34
Longitudinal Flow Velocity (m/s)	3.23	3.08	4.47	2.86
Lateral Flow Velocity (m/s)	1.93	2.67	2.82	3.53
Flow Altitude (m)	26.5	51.0	31.0	87.9
Flow Amplitude (db)	6.83	5.45	6.49	5.01
Sigma Value (m/s)	0.23	0.18	0.23	0.24
Velocity Width (Spread)(m/s)	0.39	0.42	0.52	0.36
Flow Velocity Magnitude (m/s)	3.11	3.04	4.28	3.17

5.2 Ground Truth Data

The bulk of the ground truth data on which detailed analysis was performed was obtained from the 50 meter Department of Energy meteorological tower located just north and east of the San Gorgonio pass exit, near the Southern California Edison Utility's Devers Substation. Other ground truth data was taken at a Southern California Edison 100 m tower located in the pass where hourly wind speeds from the 10 meter and 100 meter levels were provided by Aerovironment, Inc. under contract to the Southern California Edison Utility.

Additional ground truth data was obtained from three 5 meter towers and three tala kite anemometers at a height of 100 meters. This ground truth data was collected on July 10, when the first ADLS tests were performed. Since little ground truth data was taken on July 29 when the best ADLS data was collected, the July 10 ground truth data was used to develop the turbulence and mean wind profiles expected under synoptic conditions similar to the July 10 synoptic conditions. The synoptic conditions for July 29 were virtually identical to those of July 10 and thus scaling laws developed from the July 10 data were felt to be valid for the July 29 test.

The vertical variation of wind speed may be represented by coefficient, α, in the well known power law relation:

$$\frac{U_1}{U_2} \left(\frac{Z_1}{Z_2} \right)^{\alpha}$$

where V_i is the velocity at a height above grade of Z_i.

The following table represents the power law coefficients obtained at various locations as a function of time of day.

As can be seen from the data, the power law coefficient is larger near the ground and decreases with altitude. This is attributed to the flow not being a fully developed boundary layer flow but rather dominated by the influence of the acceleration through the pass. Thus upper air velocities, until the accelerated flow depth is reached, are not expected to greatly exceed those observed at the 100 meter level. This is consistent with the results obtained by the ADLS.

TABLE 5. SUMMARY OF POWER LAW COEFFICIENTS (α)

Time	50m Tower	100m Tower	Tala Kite
1500-1600	0.11	0.08	--
1529-1538			-0.01
1555-1605			0.06
1600-1700	0.13	0.11	
1625-1635			0.04
1655-1705			0.07
1725-1735			0.06

The measurements from DOE 50m tower were used for detailed analysis of near surface data. Specifically the detailed ground truth was used to estimate the turbulence levels that would be observed if an investigator were able to measure the spatial variations in a length of atmosphere similar to the focal volume of the ADLS. This was accomplished by using Taylor's hypothesis for changing a time history to a space history. That is, by multiplying a time history by the mean wind speed such that a particular quantity is related to a specific distance rather than a specific time (i.e., $X = Ut$). It was most convenient to compute temporal statistics for specific time intervals and relate them to the spatial interval through Taylor's hypothesis. This data is presented in Table 6.

The data shows that σ_u decreases with elevation and increases with sampling length. Both of these items are as expected. The σ_u decreases with elevation due to the fact that dissipation is occurring as the turbulence moves away from the boundary as well as the fact that the turbulence integral scale increases away from the boundary thereby shifting the frequency spectrum to the left. That is, there becomes less energy available in the spectral region measured by the spatial or temporal record.

This data tends to bound the turbulence data expected to be observed in the ADLS data. That is, values of σ_u in excess of 1.5 m/s would be highly suspect. Also turbulent intensities above about 0.1 would also be highly suspect. Additional data concerning the frequency distributions of the individual statistics are available from the authors by request.

The synoptic weather patterns for July 10 and July 29 were compared and showed surprising similarity.

The predominant factor that causes strong, persistent winds in the San Gorgonio Pass area during this time of year is the pressure gradient established across the pass due to cool marine air penetrating from the west and the warm air over the Mojave desert. On synoptic weather charts, the data density is too sparse to show the existence of the pressure gradient in any detail. However, the surface charts do indicate when this condition can exist by the presence of a strong Pacific Maritime high pressure system to the west

TABLE 6. AVERAGE-MEAN, RMS TURBULENT INTENSITIES FOR VARIOUS ELEVATIONS AND TIME INTERVALS (APPROXIMATE SPACE INTERVALS)

Sampling Interval	Approx. Spatial Interval (m)	Lower			Mid			Upper			Number of Data Sets
		$\overline{U}$ (m/s)	u (m/s)	$(u/\overline{u})$	$\overline{U}$ (m/s)	u (m/s)	$(u/\overline{u})$	$\overline{U}$ (m/s)	u (m/s)	$(u/\overline{u})$	
20 sec	240	11.010	1.213	0.111	12.225	0.942	0.078	13.156	0.902	0.070	496
50 sec	720	11.006	1.512	0.139	12.224	1.239	0.103	13.154	1.180	0.091	165
5 min	3,600	11.006	1.796	0.161	12.225	1.549	0.128	13.154	1.517	0.116	33
10 min	7,200	10.975	1.804	0.166	12.193	1.589	0.132	13.121	1.553	0.119	16

of the region, and a well-developed thermal low pressure system to the east of the region. Such a condition existed on July 10, as can be seen from surface weather charts on this day. Three hourly of charts, beginning with 0400 PDT (1200Z) on July 10, shows a well-developed high pressure system several hundred miles to the northwest of the region, and a closed thermal low immediately to the east of the region. During the time of the flight, (approximately 1530-1630 PDT), the pressure gradient across the region dropped from 1012 mb in Los Angeles to 1005 mb in the desert to the east of San Gorgonio, as can be seen on a 0000Z, July 11, surface chart. Since the San Gorgonio mountain range provides a physical barrier to the two air masses, it can be anticipated that this is the approximate pressure gradient that existed across the pass on that day.

Similar synoptic conditions existed on July 29. Although the center of the Pacific high pressure system is further to the north and east. The thermal low is equally well developed as it was on the 10th, as a result: the pressure gradient during the time of maximum heating (1700 PDT) was equivalent to the 10th dropping from 1012 mb in Los Angeles to 1004 mb in the desert.

The upper air charts should also provide an indication of the similarity between the two period, since the semi-permanent Pacific high pressure system shows as a ridge aloft. However, in the southwestern U.S., during the summer, upper air charts normally exhibit weak gradients. During this time the region is relatively free of synoptic-scale disturbances, and temperature differences are generated primarily by surface heating and cooling patterns, which are not reflected very strongly in upper level charts. As a result, upper level winds are generally quite light in this region during this time of year.

The 850 mb charts for July 10 indicate the weak upper-level flow conditions in the San Gorgonio region. Winds are quite light at Los Angeles, and temperature and height gradients are very weak. Temperatures at this height are about 23°C. The height of this pressure surface is about 1515 m in this region. A weak west-to-east gradient is evident associated with the Pacific high pressure system centered about 1500 miles to the northwest, and the thermal low centered over northern Mexico. In the afternoon, this gradient tightens and winds increase due to increased surface heating on the

east side of the pass. The same pattern prevailed on the 29th, only with a stronger temperature gradient evident to the north of the region associated with a large upper-level low pressure system passing across the Pacific Northwest. However, over the pass, temperatures and heights of the pressure level are nearly identical to the 10th, with a general west-east pressure gradient associated with a Pacific high pressure 2000 miles to the northwest, and a thermal low pressure over central Mexico.

Examination of the 500 mb charts reveals the synoptic conditions that prevailed over the northern hemisphere for these two time periods. The 500 mb charts for these days showed that the synoptic situation for the two periods was very similar. In both cases a low pressure trough existed over the Pacific Northwest, with temperatures at this pressure level around -20°C, and heights of the pressure level around 5700 m. Over the Pacific Southwest, temperatures on both days were about -5°C, and heights of the pressure level about 5900 m. As with the other charts, the ridge of high pressure over the Pacific Ocean appears to be somewhat closer to the mainland on the 10th than on the 29th. In addition, despite similar height gradients, winds at the 500 mb level on the 10th are much stronger, and from the southwest, than on the 29th where winds at Los Angeles were light and from the north.

In summary, examination of the surface and upper air charts for the two study periods, July 10 and July 29, show that synoptic conditions were quite similar for the two days. The Pacific high pressure system was centered closer to the coastline on the 10th than on the 29th, resulting in slightly stronger synoptic flow on the 10th. This could be reflected at San Gorgonio Pass by higher afternoon winds on the 10th than on the 29th, although the synoptic pattern supports strong thermal gradient winds across the pass for both periods.

6.0 CORRELATION ANALYSIS AND RESULTS

The same regions which were analyzed for the detailed wind vector analysis (Section 5.0) were used to compute auto-correlations for the lateral and longitudinal wind components. These correlations were then used to evaluate integral length scales. To compute the auto-correlations, the longitudinal and lateral flow directions were evaluated as a spatial average over the region of interest. Velocity components and their respective coordinates were rotated to a coordinate system such that the mean flow direction became the "X" axis or the longitudinal axis and the normal to the mean flow direction became the "Y" axis or the lateral axis. The computational procedure used to obtain the average autocorrelations from the flow field velocity components is discussed below and illustrated in Figure 9.

Each wind vector then was separated into its longitudinal and lateral component. The flow region of interest was then divided into 100 meter wide strips normal to the mean flow direction for lateral direction computations (i.e., lateral component-lateral direction and longitudinal component-lateral direction) and 100 meter wide strips parallel to the mean flow direction for longitudinal direction computations (i.e., longitudinal component-longitudinal direction and lateral component-longitudinal direction). The velocity data in each 100 meter wide strip are then interpolated using a cubic spline to provide uniformly spaced velocity data needed to perform the correlation computations. These correlations are then ensemble averaged over the region of interest producing a true spatial averaged correlation at these upper air levels.

These average auto correlations from flow over Palm Springs and the flow exiting the of San Gorgonio Pass are shown in Figures 10 to 25.

Figures 10, 11, 18, 19, 22, and 23 are computed autocorrelations for velocity components correlated in their component direction (e.g., longitudinal component - longitudinal direction). From the Fourier Integral for the autocorrelation of a velocity component in the direction of the

component $R_i(X)_i = \int_{-\infty}^{\infty} A_i(k) e^{ikX_i} dk$, and continuity one can show that with an infinite record the auto correlation should remain positive. However, for a finite record where the mean is removed from the data (as it is for correlation/covariance computation) the average value of the auto correlation may be written as:

$$\frac{1}{X} \int_0^X R(X)dX = \frac{1}{X} \int_0^X \sum_{k=1}^{\infty} A(k) \cos kX \, dX$$

which may be shown to be equal to zero when integrated over the total correlation lag X. This is because only finite harmonics remain whose correlations are harmonics of precisely the same wavenumber and thus each harmonic integrates to a value of zero over the spatial record length. Thus, for finite record lengths the integral of the correlation must equal zero if integrated to the record length. An identical analogy exists for temporal data. Thus, the negative portion of the auto correlation for the correlation of in line components using a finite record length is a necessity. The only major problem this poses is how to determine the Taylor integral length scale. The author's of this paper opted for computing the integral scale by integrating to the first zero, as will be discussed in the next section.

The interpretation of the correlations presented in Figures 10 to 25 do reveal some interesting observations. These are that in the pass region where the flow is dilitating there is little difference between in line component correlations and the correlations of components normal to their vector direction. This shows that the flow in region may not be considered isotropic. The correlations over Palm Springs appear more normal but still do not indicate isotropic flow. Longitudinal and lateral spatial correlations developed for isotropic turbulence using the Van Karmon, Kaimal or Dryden Spectrum indicate more radical differences in the longitudinal and lateral correlations that were observed near San Gorgonio.

General Autocorrelation Computational Procedure

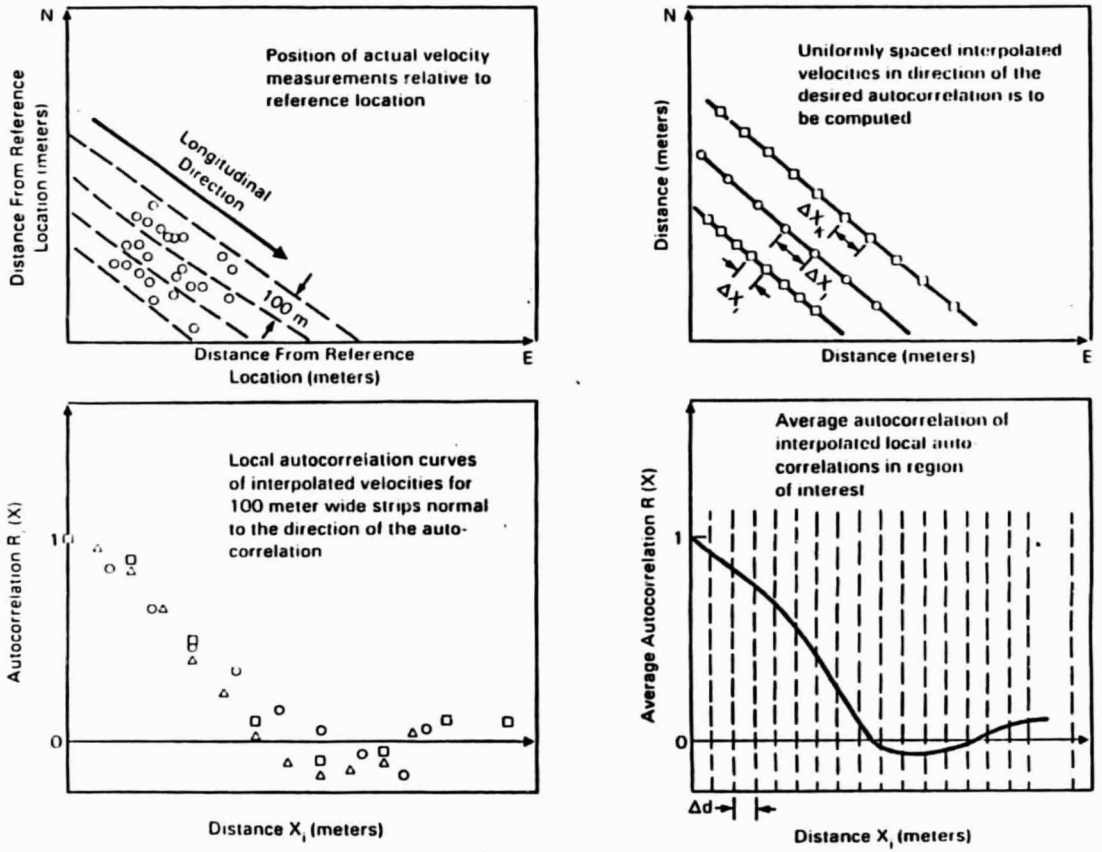

Figure 9. Correlation Procedure

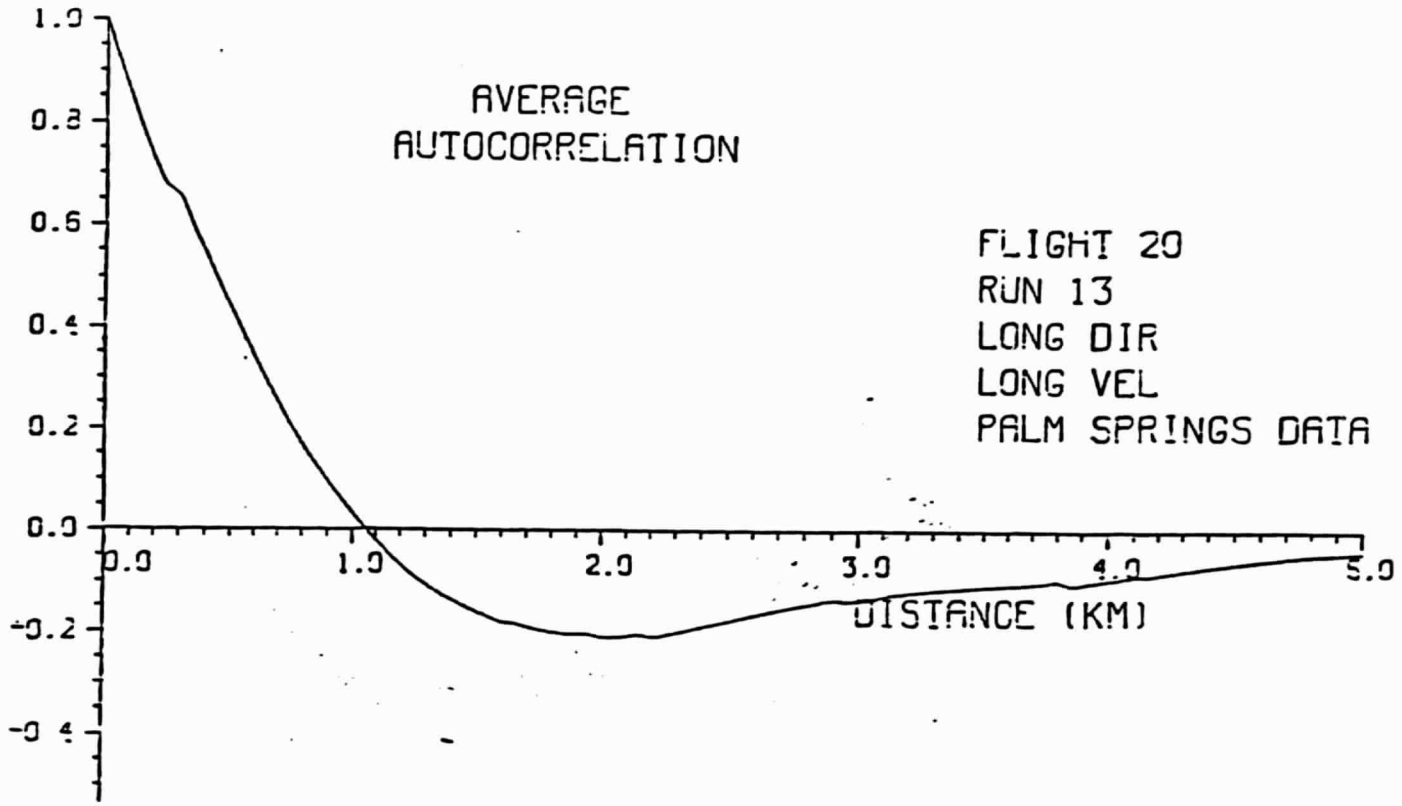

Figure 10. Average Autocorrelation of Longitudinal Component in the Longitudinal Direction over Palm Springs (Flight 20, Run 13, Elevation 650m)

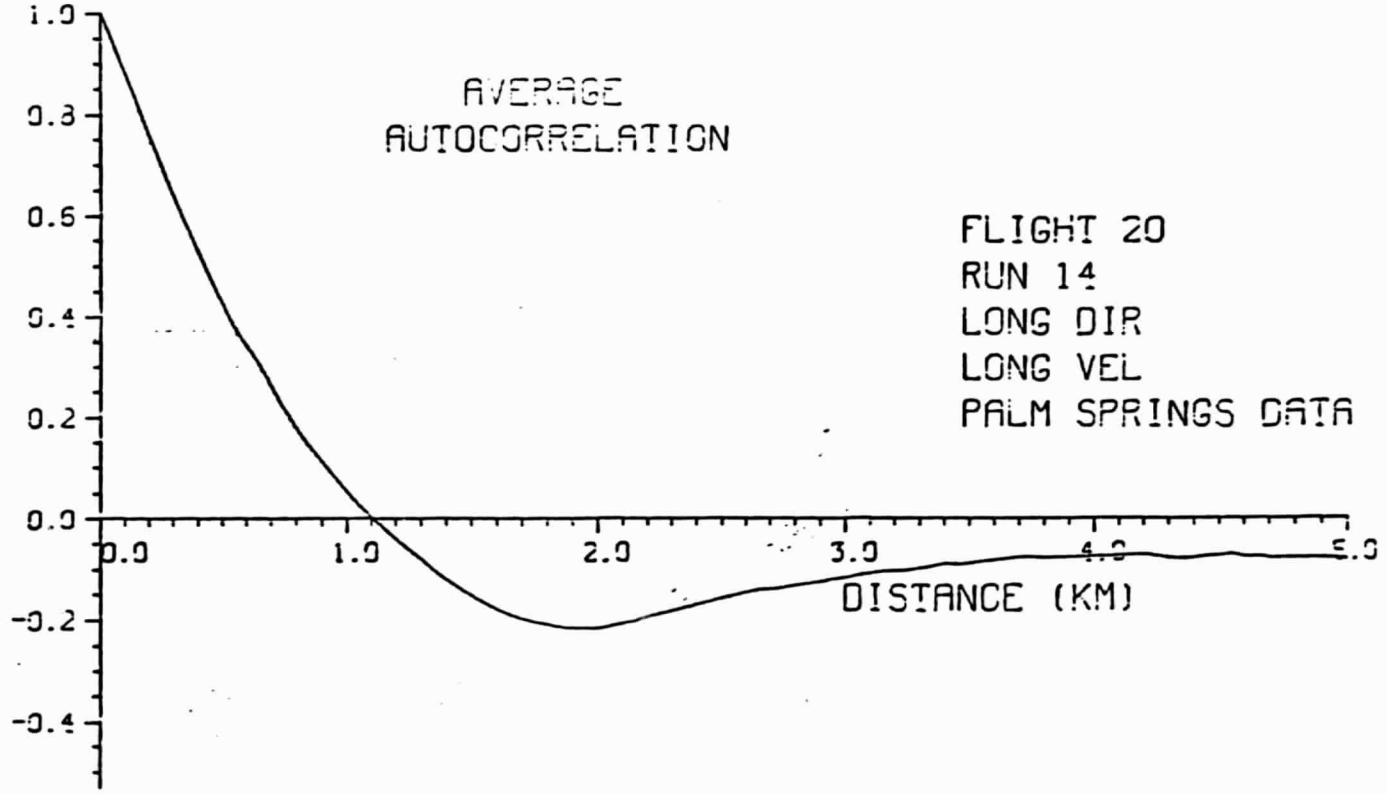

Figure 11. Average Autocorrelation of Longitudinal Component in the Longitudinal Direction over Palm Springs (Flight 20, Run 14, Elevation 800m)

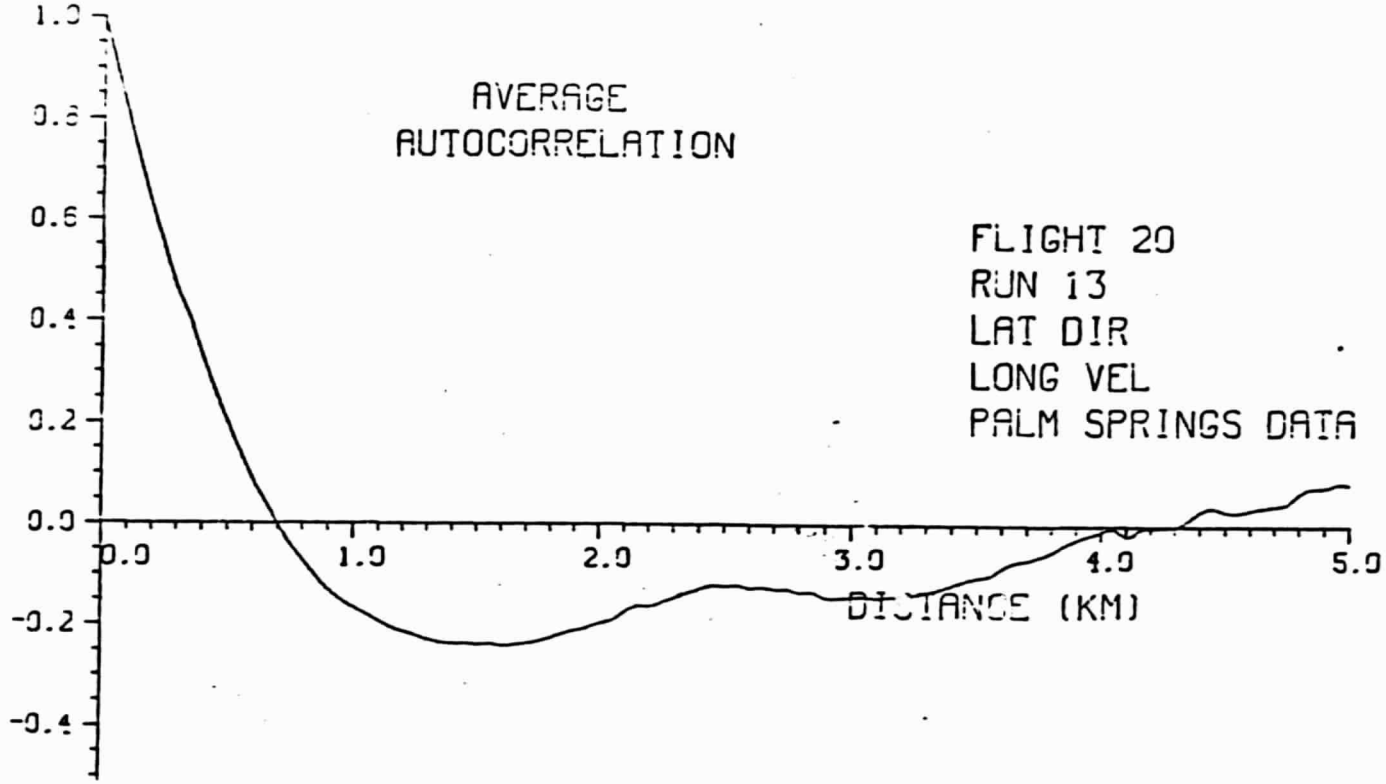

Figure 12. Average Autocorrelation of Longitudinal Component in the Lateral Direction over Palm Springs (Flight 20, Run 13)

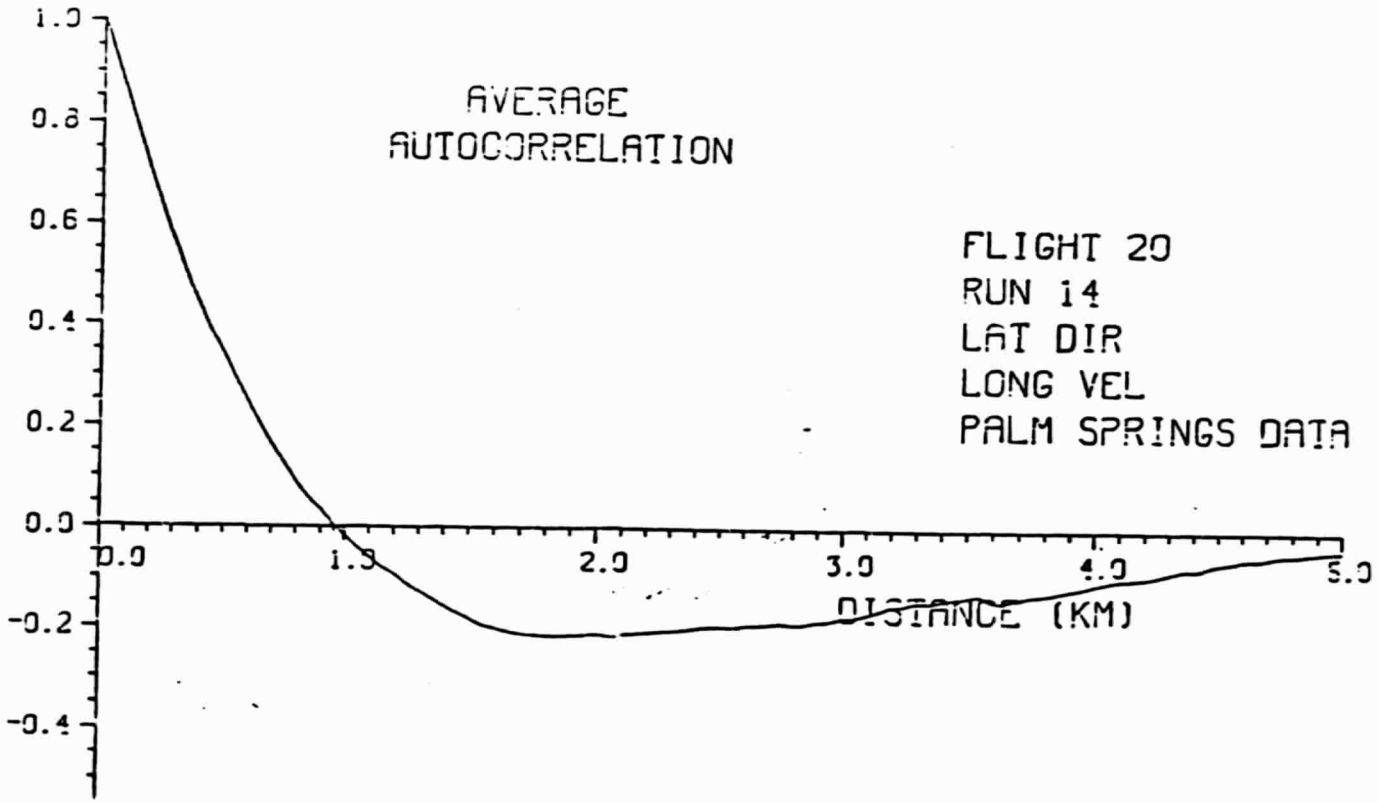

Figure 13. Average Autocorrelation of Longitudinal Component in the Lateral Direction over Palm Springs (Flight 20, Run 14)

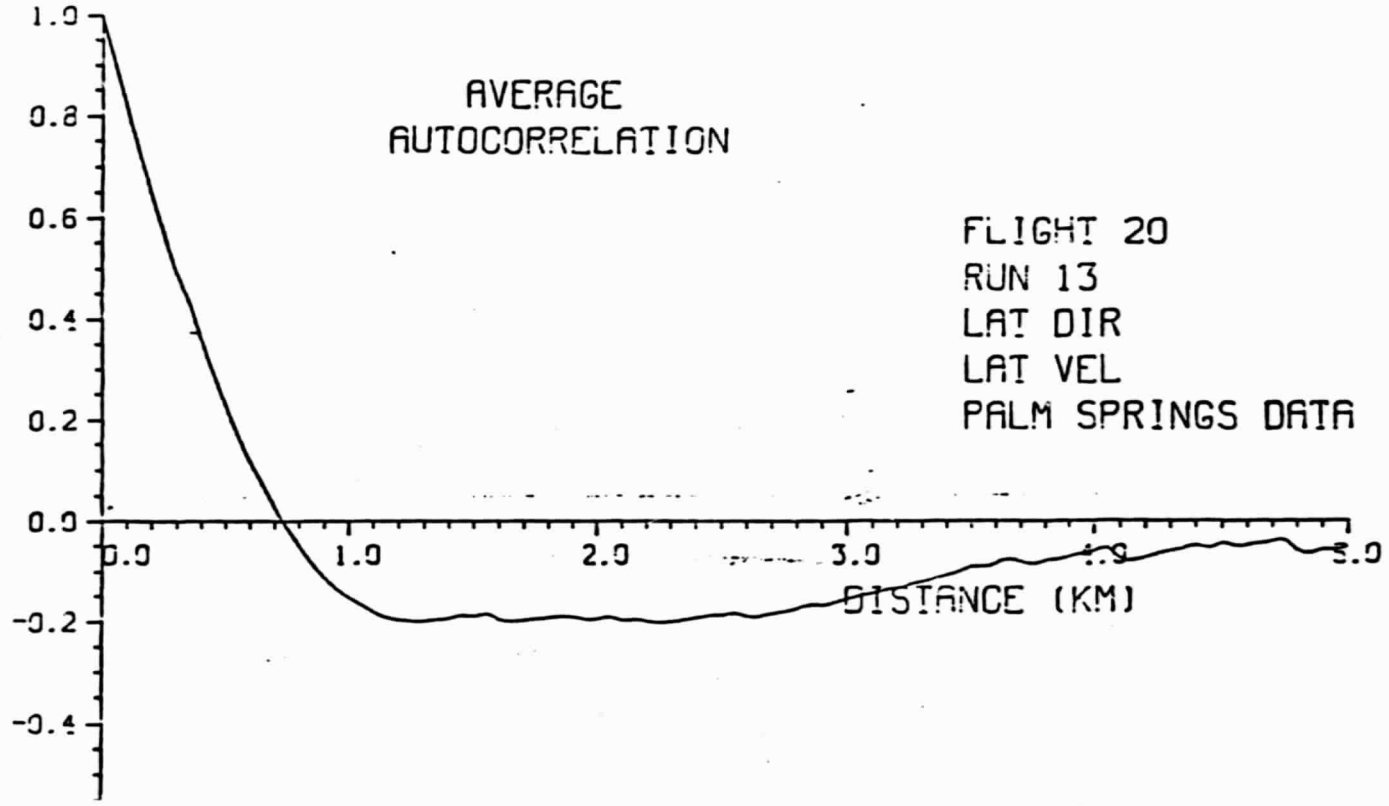

Figure 14. Average Autocorrelation of Lateral Component in the Lateral Direction over Palm Springs (Flight 20, Run 13)

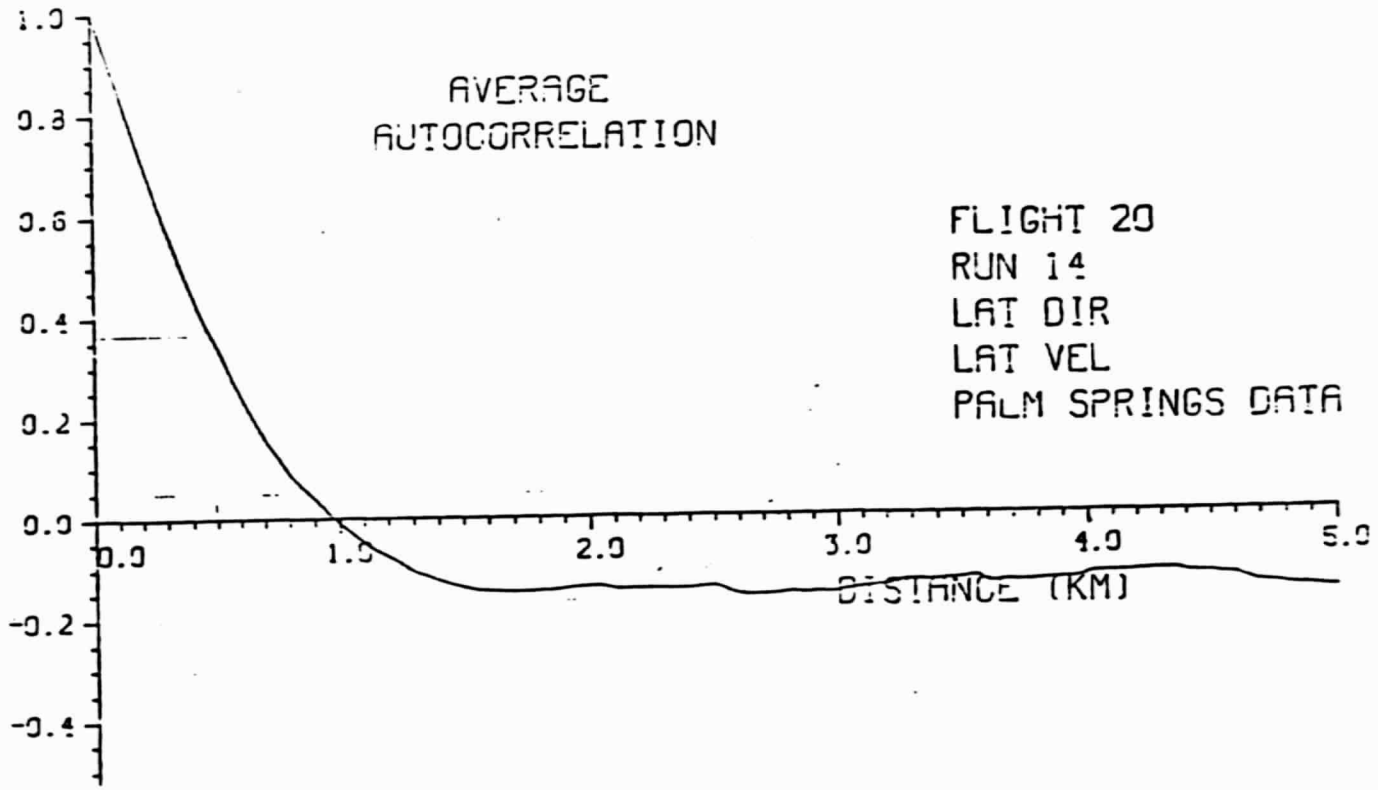

Figure 15. Average Autocorrelation of Longitudinal Component in the Lateral Direction over Palm Springs (Flight 20, Run 14)

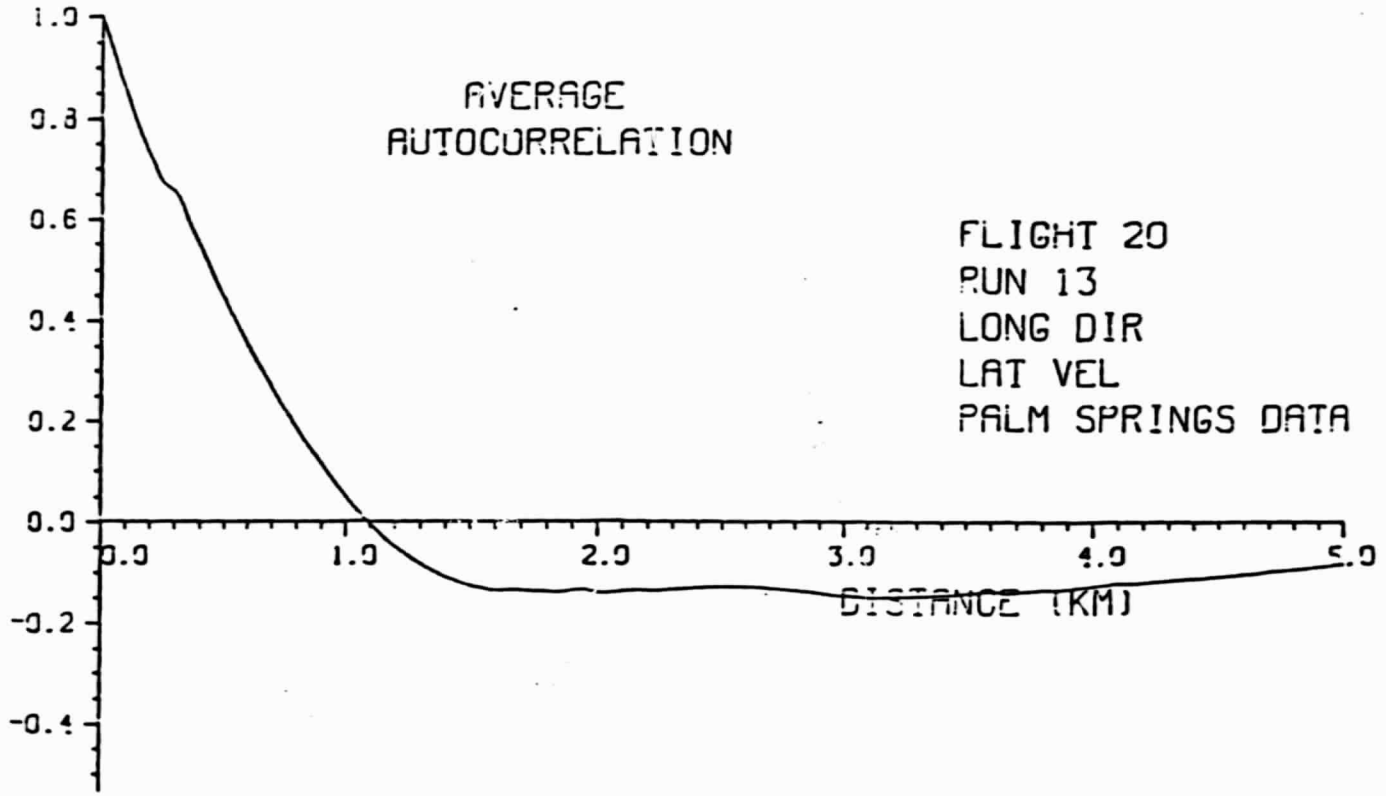

Figure 16. Average Autocorrelation of Lateral Component in the Longitudinal Direction over Palm Springs (Flight 20, Run 13)

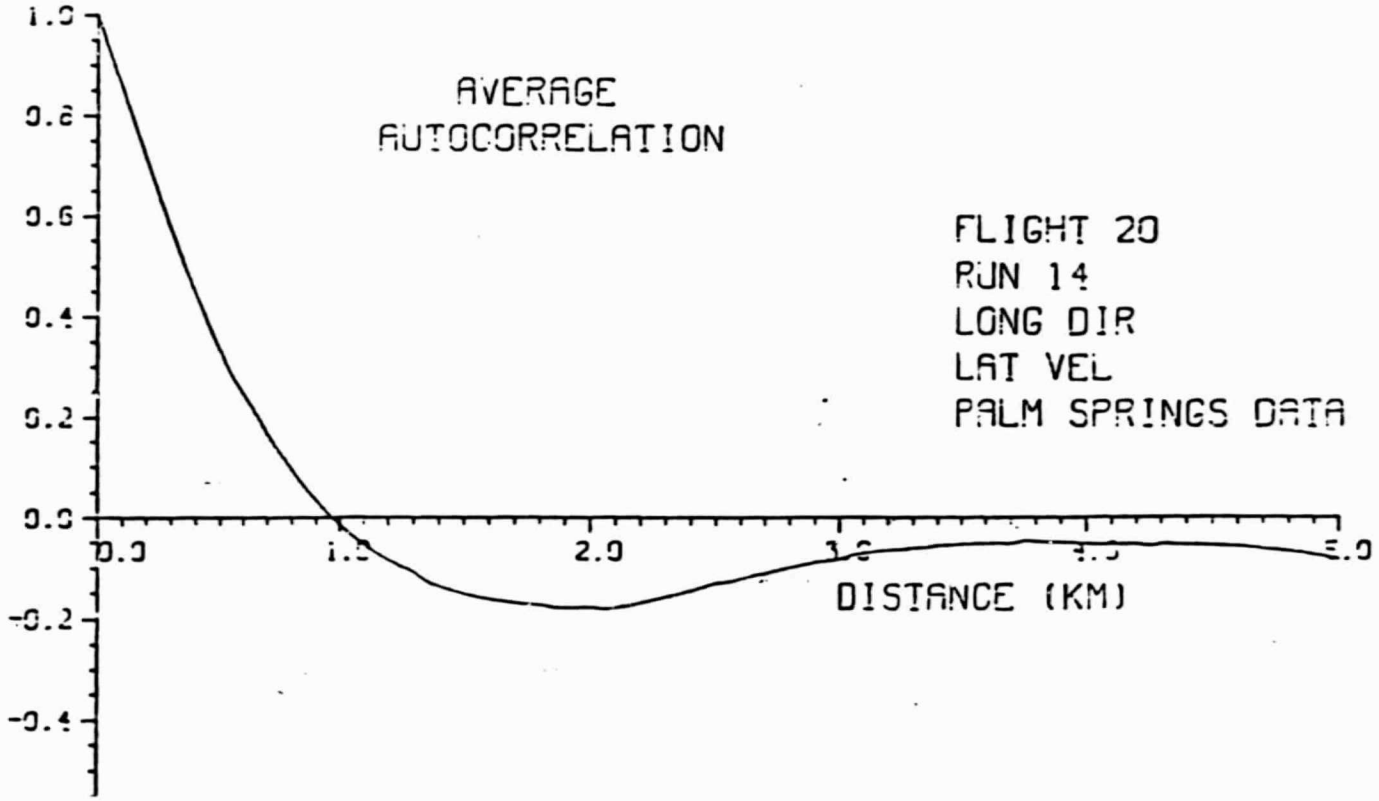

Figure 17. Average Autocorrelation of Lateral Component [illegible]he Longitudinal Direction over Palm Springs (Flight 20, Run 14)

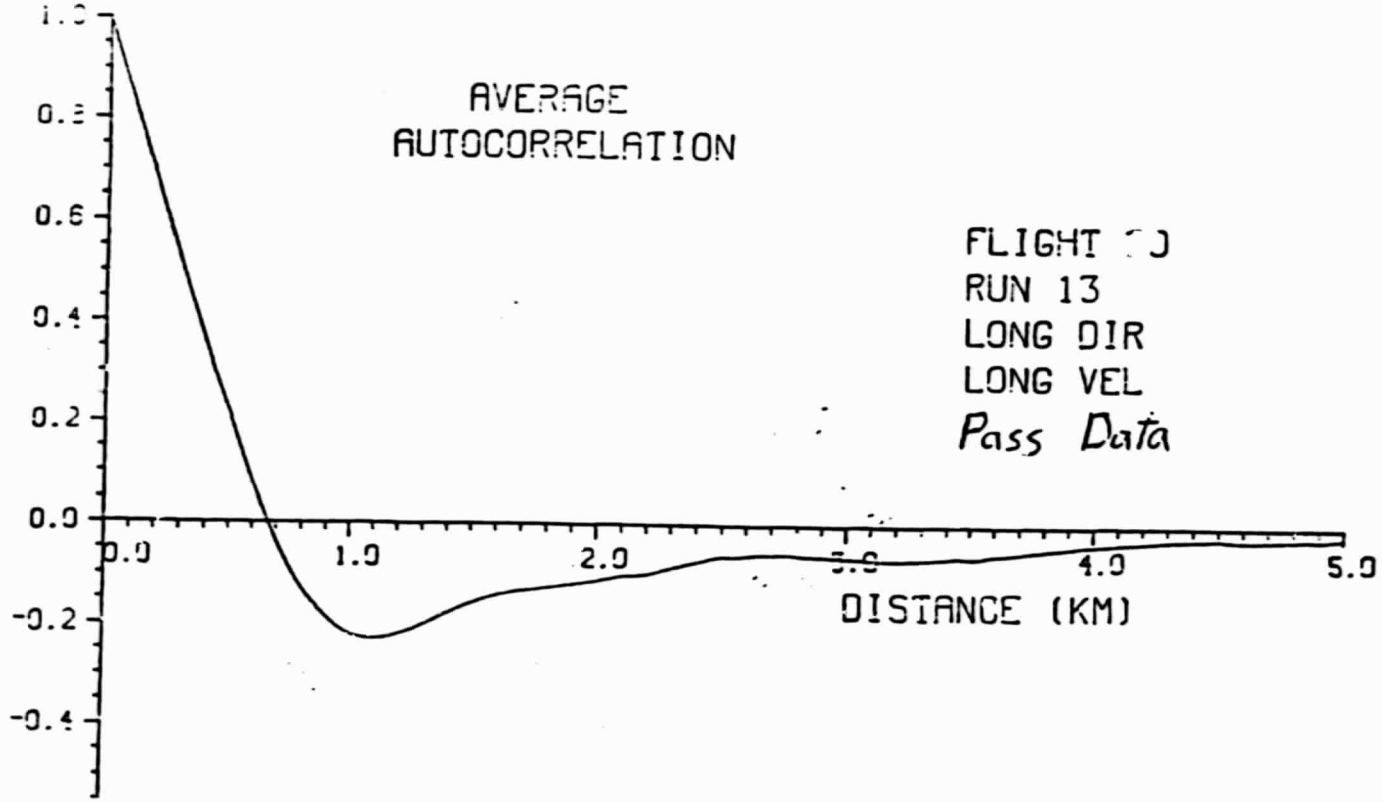

Figure 18. Average Autocorrelation of Longitudinal Component in the Longitudinal Direction over San Gorgonio Pass Exit (Flight 20, Run 13)

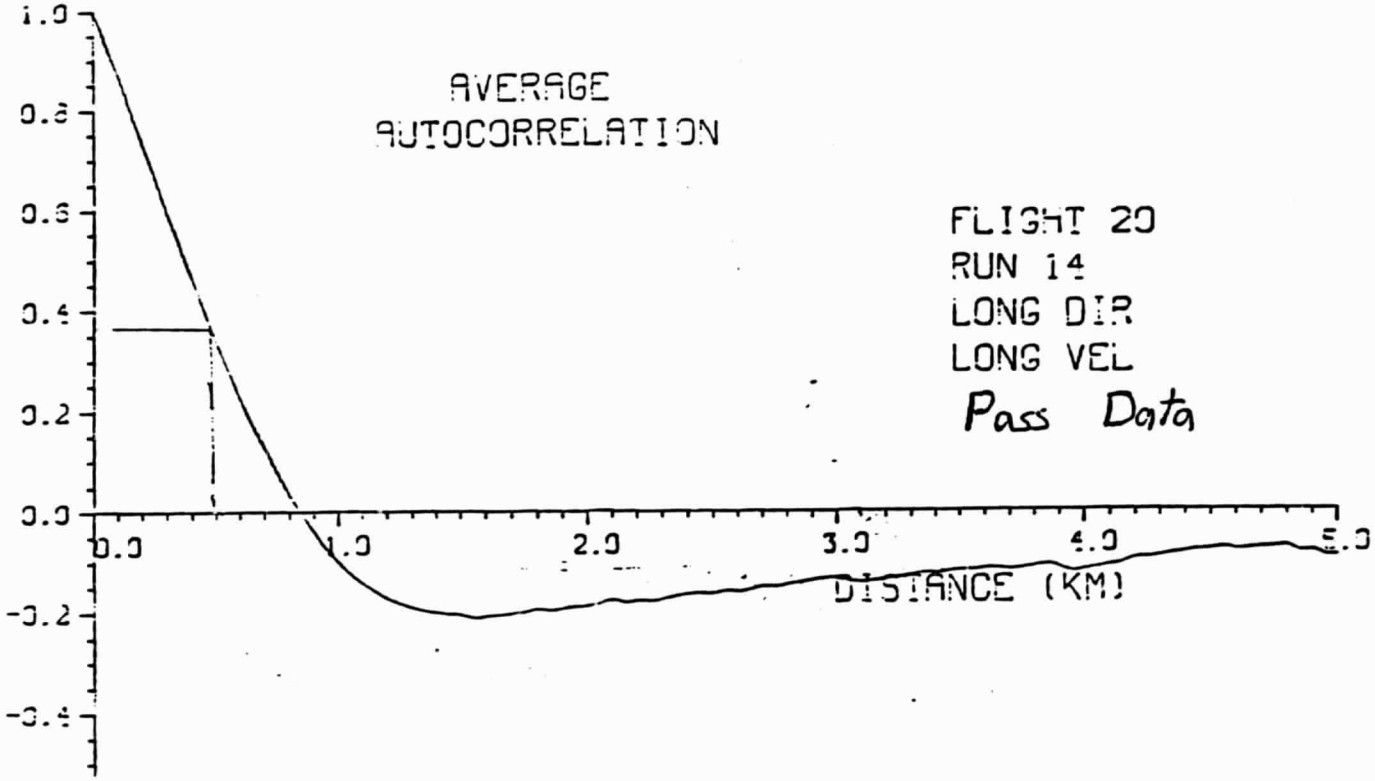

Figure 19. Average Autocorrelation of Longitudinal Component in the Longitudinal Direction over San Gorgonio Pass Exit (Flight 20, Run 14)

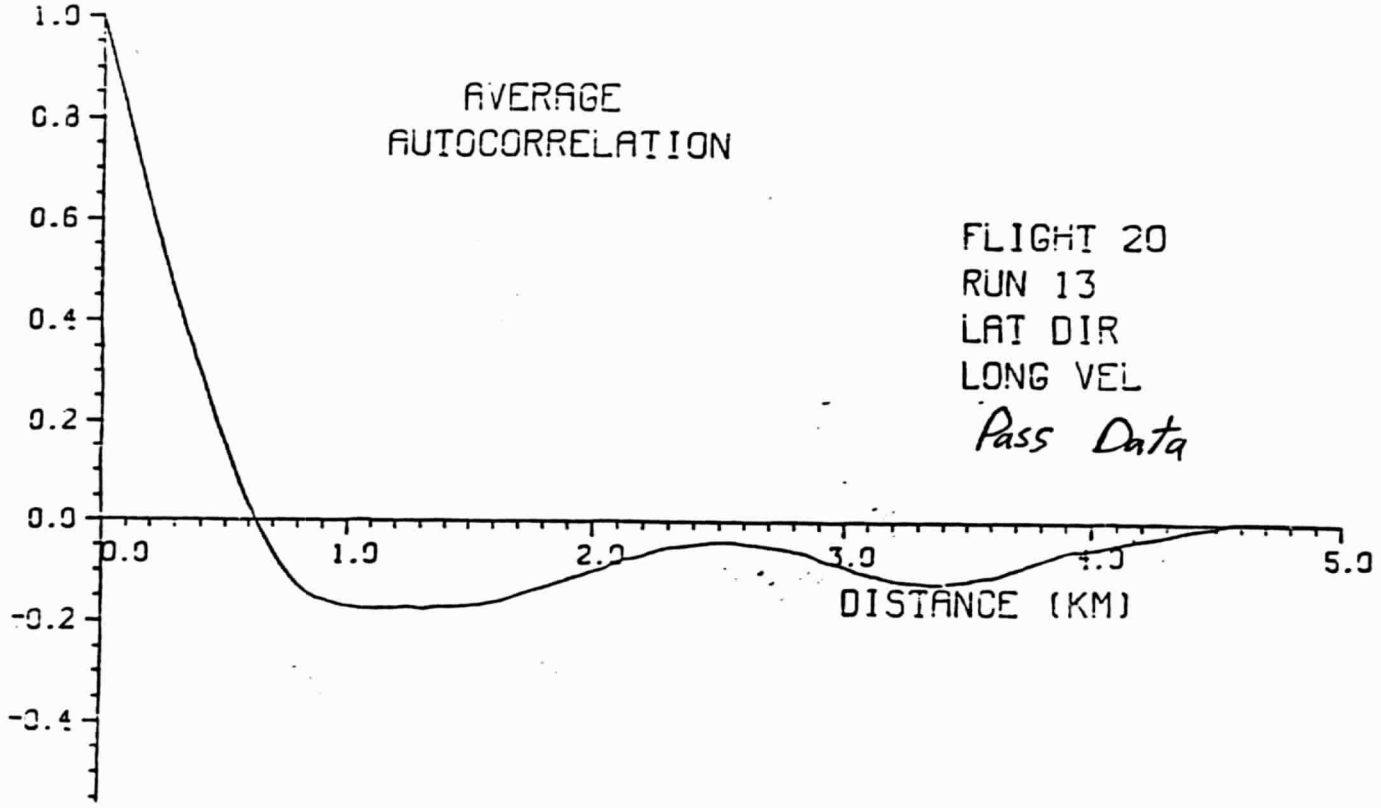

Figure 20. Average Autocorrelation of Longitudinal Component in the Lateral Direction over San Gorgonio Pass Exit (Flight 20, Run 13)

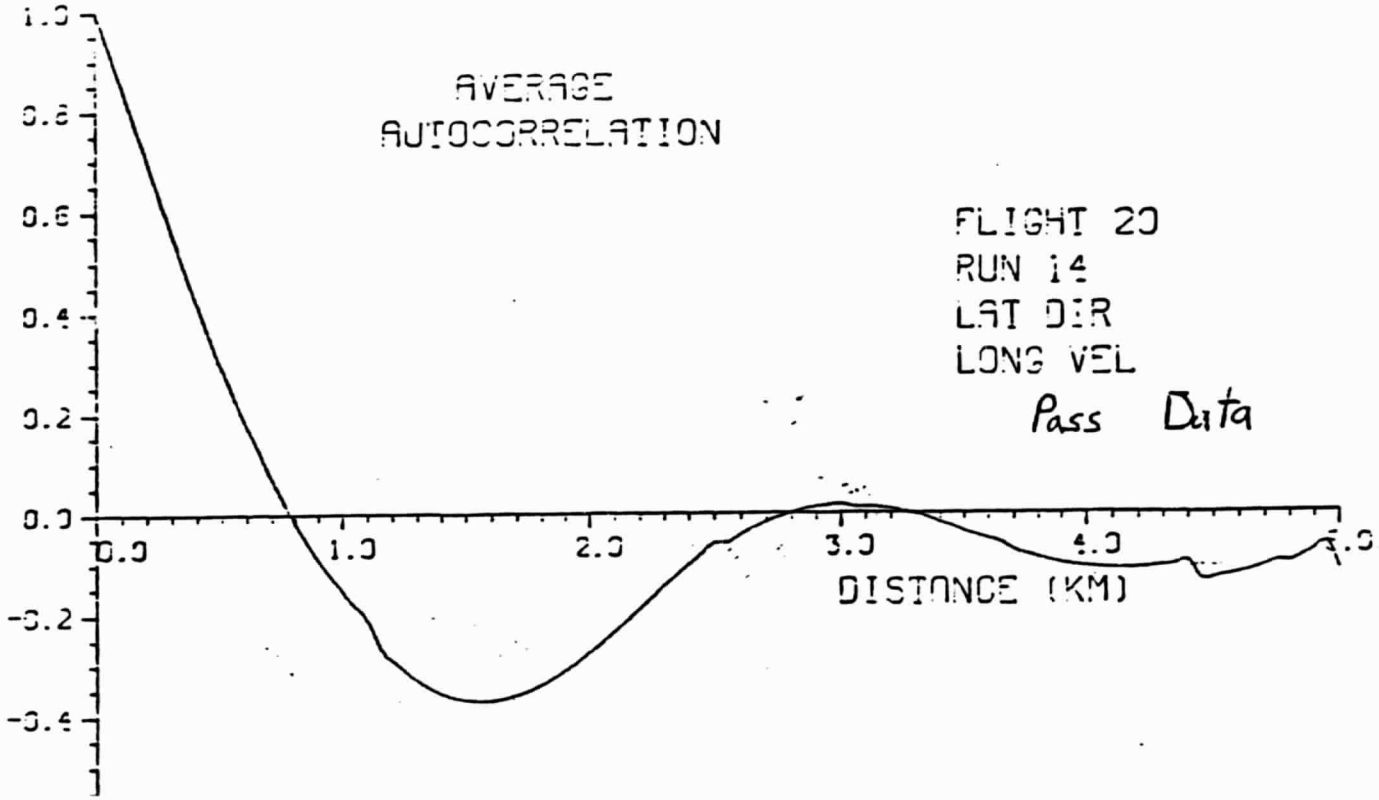

Figure 21. Average Autocorrelation of Longitudinal Component in the Lateral Direction over San Gorgonio Pass Exit (Flight 20, Run 14)

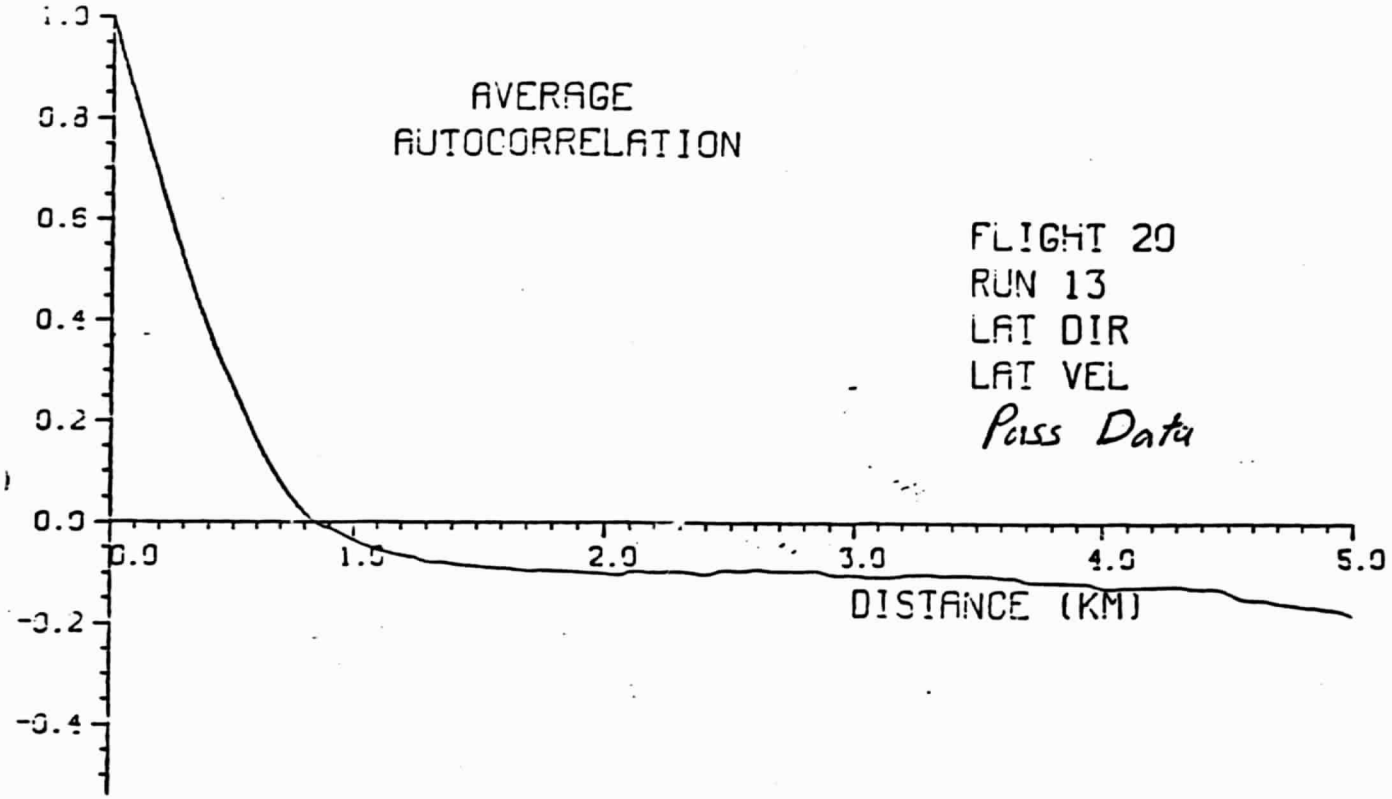

Figure 22. Average Autocorrelation of Lateral Component in the Lateral Direction over San Gorgonio Pass Exit (Flight 20, Run 13)

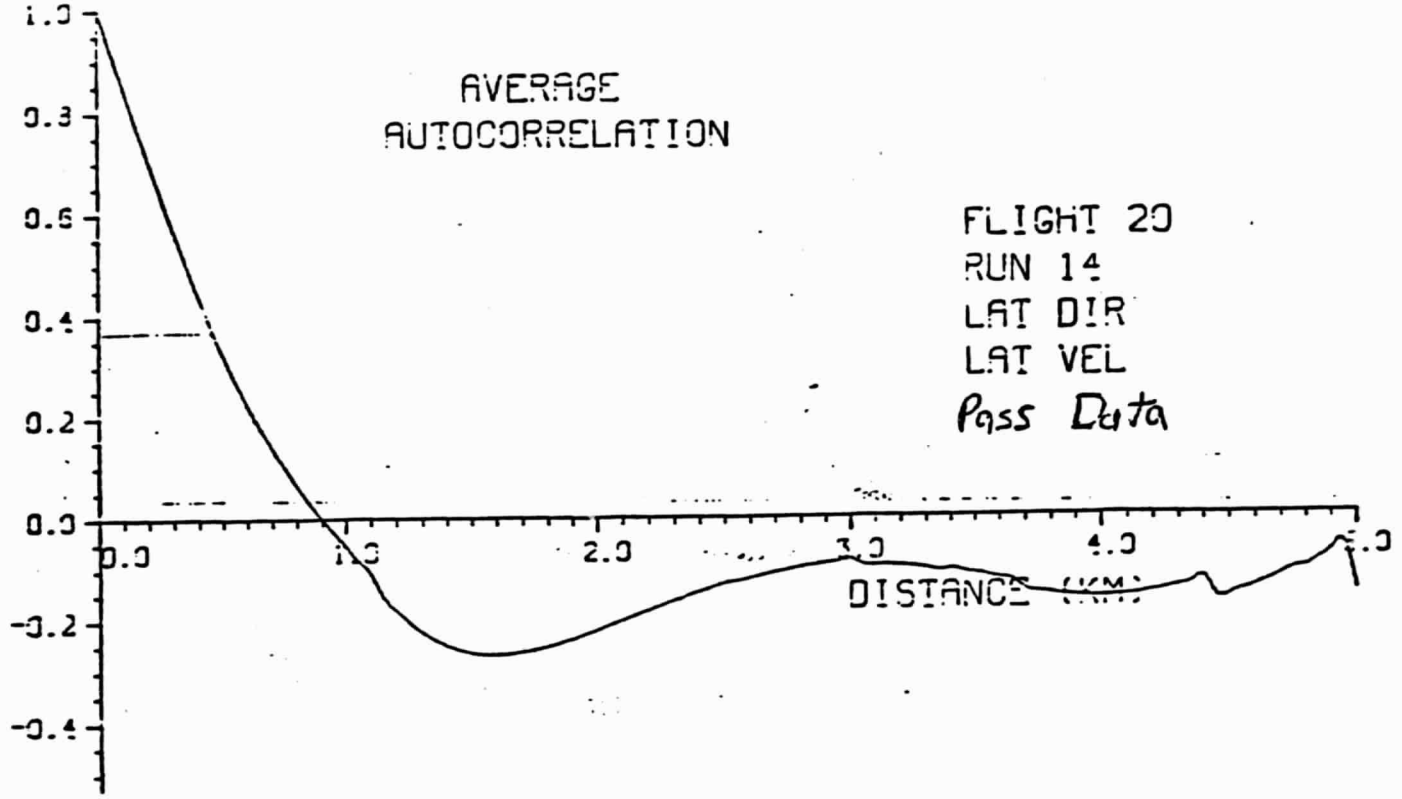

Figure 23. Average Autocorrelation of Lateral Component in the Lateral Direction over San Gorgonio Pass Exit (Flight 20, Run 14)

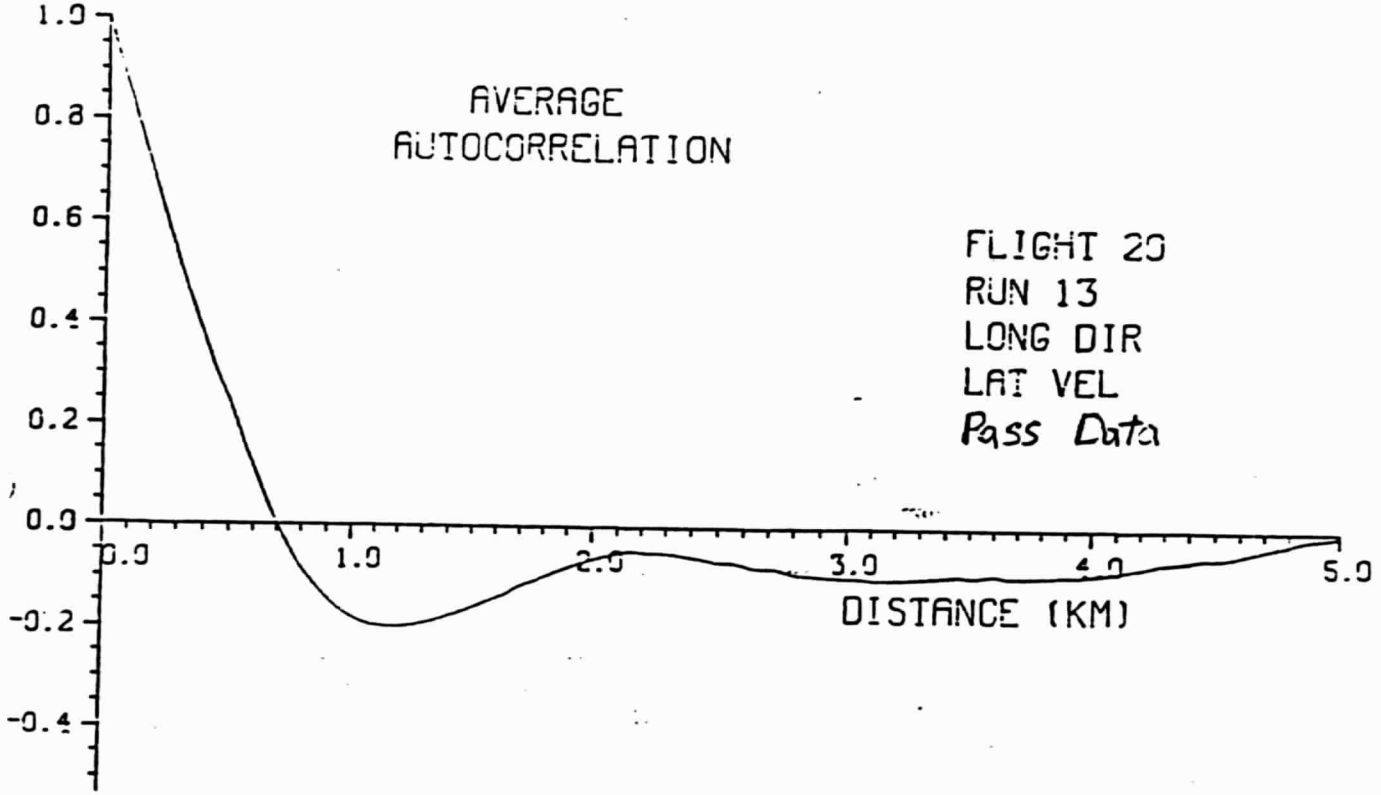

Figure 24. Average Autocorrelation of Lateral Component in the Longitudinal Direction over San Gorgonio Pass Exit (Flight 20, Run 13)

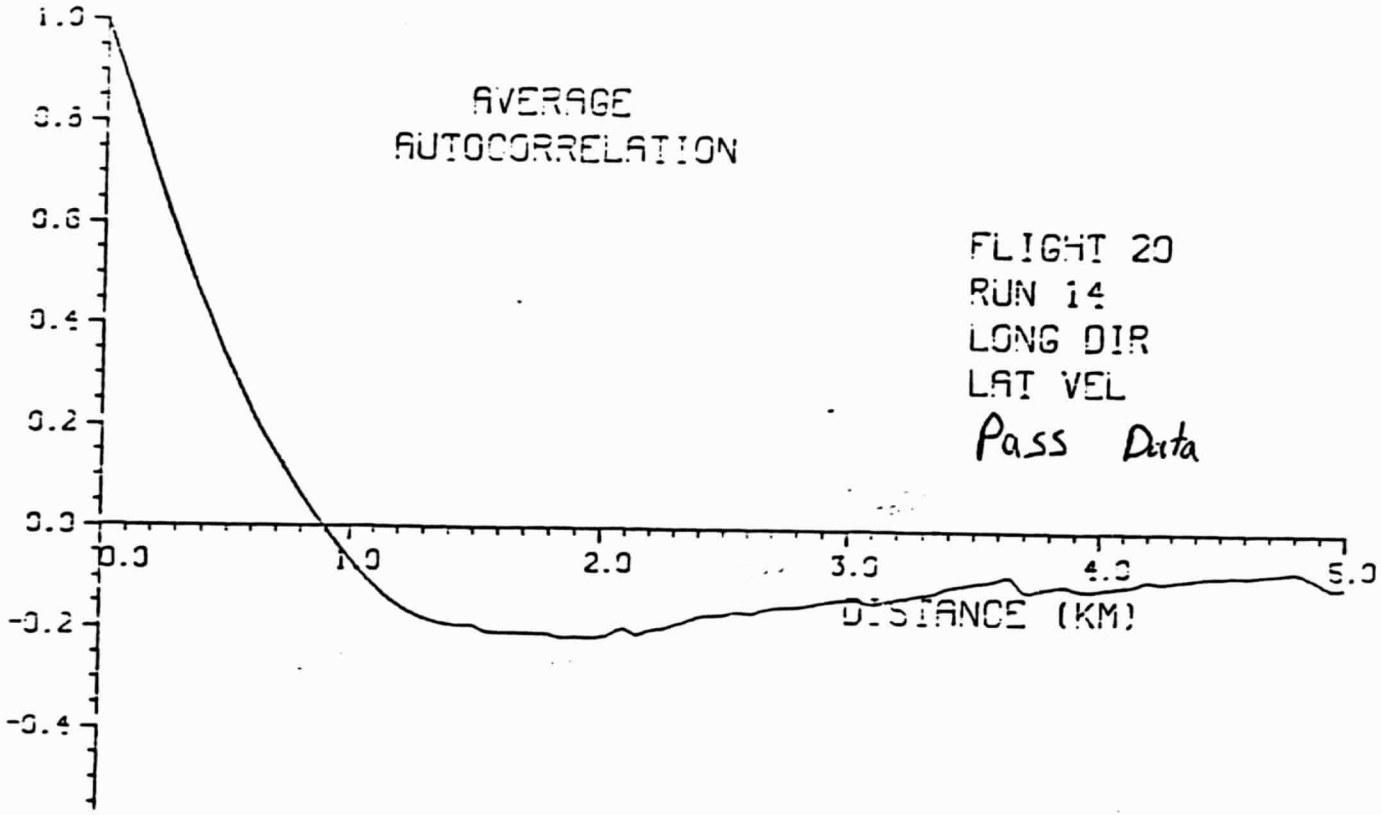

Figure 25. Average Autocorrelation of Lateral Component in the Longitudinal Direction over San Gorgonio Pass Exit (Flight 20, Run 14)

7.0 ATMOSPHERIC LENGTH SCALES

The autocorrelations provided in Section 6 were used to compute integral length scales for the flow measured over Palm Springs and at the San Gorgonio Pass exit. These length scales were computed by integrating the autocorrelation functions to their first crossing. The integral length scale was first introduced by G. I. Taylor[3] in his classical paper on "The Spectrum of Turbulence". If one examines the relations between correlation and spectra

$$R(X) = \int_{-\infty}^{\infty} A(k) e^{ikx} dk$$

and

$$A(k) = \frac{2}{4\pi} \int_{-\infty}^{\infty} R(X) e^{-ikx} dx$$

one sees that the integral length scale is simply 2π times the spectral amplitude at a wavenumber = 0.

Table 7 lists the integral length scales computed from the autocorrelations given in Section 6. Table 7 also gives estimated values of integral scales from various guideline reference documents.

TABLE 7. INTEGRAL LENGTH SCALES

Correlation Component	Correlation Direction	Integral Length Scales (Meters) Run 13 (Palm Springs)	Run 14 (San Gorg.Pass)	Counihan[5]	ESDU[6]	NASA[8]
Longitudinal	Longitudinal	465	472	273	300	762
Longitudinal	Lateral	302	400			
Lateral	Longitudinal	465	398		154	
Lateral	Lateral	320	400			

LITERATURE CITED

1. H. Yeh, and H. Z. Cummins; Localized fluid flow measurements with He-Ne laser spectrometer. Appl. Phys. lett. 4,176,1964

2. J. Bilbro, G. Fichtl, D. Fitzjarrald, M. Krause and R. Lee; Airborne Doppler Lidar Wind Field Measurements; Bulletin of the American Meteorological Society, Vol. 65, No. 4, April 1984.

3. G. I. Taylor; The Spectrum of Turbulence, Proceedings of the Royal Society, A, Vol. CLXIV (1938), pp. 476-490.

4. J. W. Bilbro and William W. Vaughan; Bulletin of the American Meteorological Society, Vol. 59, No. 9, September 1978.

5. J. Counihan; "Adiabatic Atmospheric Boundary Layers: A Review and Analysis of Data From the Period 1880-1972; Atmospheric Environment; Vol. 9, pp. 871-905, 1975, Great Britian.

6. "Characteristics of Atmospheric Turbulence Near the Ground - Part II: Single Point Data for Strong Winds (Neutral Atmospheric)". Engineering Science Data Unit, Item No. 74031, March 1975.

7. "Characteristics of Atmospheric Turbulence near the Ground - Part III: Variations in Space and Time for Strong Winds (Neutral Atmospheric). Engineering Science Data Unit, Item No. 75001, October 1976.

8. "Terrestrial Environmental (Climactic) Criteria Guidelines for Use in Aerospace Vehicle Development", 1982 Revision, NASA TM 82473, Robert E. Turner and C. Kelly Hill, Compliers, June 1982.

9. R. W. Hornbeck, Numerical Methods, Quantum Publishers, Inc. New York, 1975.

APPENDIX A

TEST PLAN FOR NASA'S AIRBORNE DOPPLER LIDAR SYSTEM (ADLS) TESTING IN SAN GORGONIO PASS AREA

INTRODUCTION

During FY81, NASA/MSFC elected to perform a flight test option called "The San Gorgonio Test Option". For this test option the NASA will use its airborne Doppler Lidar System to characterize the accelerated flow region in and near San Gorgonio Pass, California. At this region the maritime layer from the west coast to accelerated through the pass and then spreads out over the valley floor on the east side of the pass. The experiment was selected in order to study accelerated flow in and at the exit of the canyon. The test will also provide information on the atmospheric flow in this region for which DOE, Southern California Edison, and the State of California have expressed interest from wind energy resource considerations.

The NASA ADLS is pulsed and has a spatial resolution of about 300 m and will average over 140 contiguous beam paths for each range gate to a range of 10 km. This system measures the along-line-of-site wind velocity component.

Ground truth will be available for limited comparison with the NASA ADLS results. The ground truth will include wind data taken, concurrently with the flight data, by

a) one 100 m (330 ft) tower, 4 levels of instrumentation (Data will be taken courtesy of Southern California Edison by Aerovironment personnel.)

b) one 50 m (160 ft) tower, 3 levels of information (Data will be taken for DOE by PNL.)

c) approximately ten meter (33 ft) towers, one level of instrumentation (Data will be taken courtesy of Southern California Edison by Aerovironment personnel.)

d) three tala kites (Data will be taken courtesy of Southern California Edison by Aerovironment personnel.)

The NASA aircraft must have an air-to-ground communication system so that the flight paths, times, etc., can be continuously communicated to the Southern California Edison, Aerovironment, and PNL personnel taking the ground truth data.

Personnel tentatively identified to coordinate the various ground truth activities are

PNL--Dave Renne or Tom Heister (509) 375-6161
Battelle--William Cliff (509) 375-2024
Southern Cal. Edison--Robert Yinger (213) 572-2196
Aerovironment--Tom Zambrano (213) 449-4329

It is expected that Battelle, PNL, and Southern California Edison will have representatives on board the aircraft during the flight testing. These personnel will require ground communication to their in-the-field personnel.

FLIGHT PATHS FOR NASA AIRBORNE DOPPLER LIDAR SYSTEM

The following flight paths have been designed to obtain information of the flow at the exit of San Gorgonio Pass and flow through the pass. These flight paths have also been designed to obtain information which may be compared with data obtained at the ground stations previously described.

Flight Path No. 1

Beam Configuration: Locked, looking forward and down

Axmuthal angle of beam, θ_A (top view) = 13.84^o

Elevation angle of beam, θ_E (front view) = 15.00^o

Vertical angle of beam, θ_Z (side view inside plane) = 47.41^o

Flight Path: South to north along constant longitude of $116^o34'43"W$ (along section line which bisects sections 20 and 21 in Township 3S and Range 4E)

Starting at Latitude: $33^o51'35"N$
Ending at Latitude: $33^o58'30"N$

Altitude of flight path: 7620 ft above sea level

This flight path is 4.8 miles from the Southern California Edison 100 meter tower. The beam will intercept the ground at the tower, thus permitting comparison with the tower measurements. This flight path will also provide data on the vertical profile of the horizontal velocity field. In this configuration each unit length of the laser beam will have a northerly component of 0.23147, a westerly component of 0.93969, and a vertical component of -1.25179.

Flight Path No. 2, 3, and 4

Beam Configuration: Same as Flight Path No. 1

Flight Path: South to north along a constant longitude of $116^o32'41"$ (directly along Indian Avenue, bisecting Sections 22 and 23 in Township 3S and Range 4E)

Starting Latitude: 33°50'44"N
Ending Latitude: 33°58'30"N

(Starting on the intersections of Sections 10, 11, 14 and 15 of Township 4S and Range 4E, and ending on the intersection of Sections 22, 23, 26 and 27 of Township 2S and Range 4E)

Altitude of Flight Path:

No. 1: 3760 ft above sea level
(This is about 3000 ft above North Palm Springs)

No. 2: 4260 ft above sea level

No. 3: 5760 ft above sea level

This flight path is 2 miles from the DOE tower and Southern California wind turbine area. These flights should help define the vertical profile in the region where the valley opens up.

Flight Paths No. 5, 6, 7, 8, 9, 10, and 11

Beam Configuration: Nominal horizontal scan

Flight Path: South to north on odd number flight paths and north to south on even number flight paths

All flights along constant longitude of 116°34'43"W
(Same as flight path No. 1)

Starting Latitude: 33°51'35"N
Ending Latitude: 33°58'30"N
(Latitudes same as Flight Path No. 1)

Altitude of Flight Paths:

No. 5: 2500 ft above seal level
(about 1500 ft above terrain)

No. 6: 2500 ft above sea level

No. 7: 3000 ft above sea level

No. 8: 3500 ft above sea level

No. 9: 3500 ft above sea level

No. 10: 6000 ft above sea level

No. 11: 6000 ft above seal level

These flights are to describe the horizontal flow field near and outside the exit of the pass.

Flight Paths No. 12, 13, 14, 15, 16, and 17

Beam Configuration: Nominal horizontal scan

Flight Path: East to west on even numbered flights and west to east on odd numbered flights.

Even numbered flights the plane should stay 1/2 mile north of Interstate 10 beginning where Interstate 10 crosses flight path No. 2 (Longitude 116°32'41") and proceed west to Banning. Odd numbered flights should stay 1/2 mile south of Interstate 10 beginning at Banning and proceeding east to where Interstate 10 crosses flight path No. 2.

All flight paths are to be slanted such that the plane stays a constant height above grade.

Height above grade for flight path:

No. 12	1500
No. 13	1500
No. 14	2500
No. 15	2500
No. 16	5000
No. 17	5000

These flight paths will be approximately 18 miles long and will define the horizontal wind field, its velocity and direction as it flows down the pass. It will also assist in defining the depth of the maritime layer near Banning.